Molecular Biology of the Cell
Vol. 21, 2756–2769, August 1, 2010

Aspergillus RabB^{Rab5} Integrates Acquisition of Degradative Identity with the Long Distance Movement of Early Endosomes

Juan F. Abenza,*† Antonio Galindo,*† Areti Pantazopoulou,* Concha Gil,‡ Vivian de los Ríos,* and Miguel A. Peñalva*

*Departamento de Medicina Celular y Molecular, Centro de Investigaciones Biológicas del CSIC, Madrid 28040, Spain; and ‡Departamento de Microbiología II, Facultad de Farmacia, Universidad Complutense, Madrid 28040, Spain

Submitted February 12, 2010; Revised May 13, 2010; Accepted June 2, 2010
Monitoring Editor: Gero Steinberg

Aspergillus nidulans **early endosomes display characteristic long-distance bidirectional motility. Simultaneous dual-channel acquisition showed that the two Rab5 paralogues RabB and RabA colocalize in these early endosomes and also in larger, immotile mature endosomes. However, RabB-GTP is the sole recruiter to endosomes of Vps34 PI3K (phosphatidylinositol-3-kinase) and the phosphatidylinositol-3-phosphate [PI(3)P] effector AnVps19 and *rabB*Δ, leading to thermosensitivity prevents multivesicular body sorting of endocytic cargo. Thus, RabB is the sole mediator of degradative endosomal identity. Importantly, *rabB*Δ, unlike *rabA*Δ, prevents early endosome movement. As affinity experiments and pulldowns showed that RabB-GTP recruits AnVps45, RabB coordinates PI(3)P-dependent endosome-to-vacuole traffic with incoming traffic from the Golgi and with long-distance endosomal motility. However, the finding that *Anvps45*Δ, unlike *rabB*Δ, severely impairs growth indicates that AnVps45 plays RabB-independent functions. Affinity chromatography showed that the CORVET complex is a RabB and, to a lesser extent, a RabA effector, in agreement with GST pulldown assays of AnVps8. *rabB*Δ leads to smaller vacuoles, suggesting that it impairs homotypic vacuolar fusion, which would agree with the sequential maturation of endosomal CORVET into HOPS proposed for *Saccharomyces cerevisiae*. *rabB*Δ and *rabA*Δ mutations are synthetically lethal, demonstrating that Rab5-mediated establishment of endosomal identity is essential for *A. nidulans*.**

INTRODUCTION

Rab5 GTPases are major determinants of early endosome (EE) identity and master regulators of endocytic traffic by recruiting, in their "GTP conformation," "effector" proteins to endosomal membrane domains. Key human Rab5 effectors, such as rabaptin-5, the PI(3)K hVps34, the hVps45 and phosphatidyl inositol-3-phosphate [PI(3)P] binder rabenosyn-5 and the tethering factor and also PI3(P) binder EEA1 were identified using affinity chromatography (Horiuchi *et al.,* 1997; Simonsen *et al.,* 1998; Christoforidis *et al.,* 1999a,b; Nielsen *et al.,* 2000). Cooperative interactions between these effectors and Rab5 and between different effectors themselves ensure their highly specific and efficient recruitment to EEs (Zerial and McBride, 2001). For example, the Rab5 guanine nucleotide exchange factor (GEF) Rabex associates with rabaptin-5, leading to a positive feedback loop (Horiuchi *et al.,* 1997), whereas GTP-Rab5 and the hVps34 product PI3(P) cooperate to recruit the FYVE domain proteins rabenosyn-5 and EEA1 [FYVE domains are decoders of PI(3)P signaling on endosomes; Burd and Emr, 1998; Gaullier *et al.,* 1998]. PI(3)P also mediates recruitment to endosomes of Vps27p/Hrs1, which plays a key role in the biogenesis of multivesicular bodies (MVBs; Bilodeau *et al.,* 2002; Katzmann *et al.,* 2003; Prag *et al.,* 2007).

In *Saccharomyces cerevisiae* three Rab5 paralogues, Ypt51p/Vps21p, Ypt52p, and Ypt53p, regulate endocytic traffic, but Vps21p plays a major role (Singer-Kruger *et al.,* 1994; Horazdovsky *et al.,* 1994). The Rabex orthologue and Vps21p GEF is Vps9p (Hama *et al.,* 1999). Vps19p (also denoted Vac1p) is a Vps21p effector that binds endosomal PI(3)P and the Sec1/Munc18-related (SM) protein Vps45p, thus coordinating PI(3)P signaling and fusion of Golgi-derived vesicles with endosomes (Peterson *et al.,* 1999; Tall *et al.,* 1999). In summary, it seems that traffic through EEs and acquisition of "degradative endosome identity" in fungi closely resembles the situation in mammalian cells. Thus, the identification of the CORVET ("class C" core vacuole/endosome tethering) complex as a key effector of *S. cerevisiae* Vps21p (Peplowska *et al.,* 2007) was an important finding. Like the HOPS (homotypic fusion and vacuole protein sorting) complex, a Ypt7/Rab7 effector involved in homotypic vacuolar fusion, CORVET contains the class C proteins, Vps11p, Vps16p, Vps18p, and Vps33p. However, these two complexes differ in that CORVET contains Vps3p and Vps8p, whereas HOPS contains Vps41p and the Ypt7p GEF, Vps39p (Peplowska *et al.,* 2007). CORVET mediates the maturation of EEs into late endosomes (LEs), a process involving EE fusion events in which Vps8 seems to play a tethering role (Markgraf *et al.,* 2009). Once endosomes reach a certain maturation stage,

This article was published online ahead of print in *MBoC in Press* (http://www.molbiolcell.org/cgi/doi/10.1091/mbc.E10–02–0119) on June 9, 2010.

† These authors contributed equally to this work.

Address correspondence to: Miguel Angel Penalva (penalva@cib.csic.es).

Abbreviations used: CORVET, "class C" core vacuole/endosome tethering; EE, early endosome; GEF, guanine nucleotide exchange factor; LE, late endosome; HOPS, homotypic fusion and vacuole protein sorting; MT, microtubule; PI(3)P, phosphatidyl inositol-3-phosphate; PI3K, phosphatidyl inositol-3-kinase; SM, Sec1/Munc18-related.

© 2010 by The American Society for Cell Biology

CORVET is substituted by HOPS, and LEs become competent to undergo fusion with vacuoles (Peplowska *et al.*, 2007).

One important feature of mammalian EEs is that they undergo Rab5-dependent movement on microtubules (MTs; Aniento *et al.*, 1993; Nielsen *et al.*, 1999; Hoepfner *et al.*, 2005). *S. cerevisiae* EEs are static, but those of the filamentous fungi *Ustilago maydis* and *Aspergillus nidulans* also undergo MT-dependent movement (Lenz *et al.*, 2006; Steinberg, 2007; Zekert and Fischer, 2008; Abenza *et al.*, 2009), making these organisms attractive genetic models to gain insight into the relationship between EE motility and maturation. These studies are notably facilitated by the fact that motile *A. nidulans* EEs can be differentiated unmistakably from relatively static LEs and from the *trans*-Golgi using standard epifluorescence microscopy (Pantazopoulou and Peñalva, 2009).

A. nidulans shows little genetic redundancy. Among its repertoire of nine Rabs, the sole example of paralogy actually corresponds to the two Rab5 homologues, RabA and RabB (Sánchez-Ferrero and Peñalva, 2006). We previously determined that RabA localizing to EEs plays a minor role in the endocytic down-regulation of a plasma membrane cargo (Abenza *et al.*, 2009). We report here that RabB, the sole recruiter to endosomes of the prototypical Rab5 effectors AnVps19, AnVps45, and AnVps34, plays the major role in endocytic degradation. We further demonstrate that motile EEs contain PI(3)P and that their long-distance movement is RabB-dependent. RabB and, to a lesser extent, RabA recruit CORVET and their null alleles are synthetically lethal. Thus RabB coordinates acquisition of degradative identity in early endosomes with incoming Golgi traffic, long distance movement and maturation of these EEs into late endosomes.

MATERIALS AND METHODS

Aspergillus *Media and Molecular Biology*

Synthetic complete medium contained 1% glucose and 5 mM ammonium tartrate unless otherwise indicated. Complete medium (MCA) was used for maintenance of *A. nidulans* strains (Supplementary Table 1). Membrane protein extraction and mouse anti α-green fluorescent protein (GFP; Roche's monoclonal cocktail, 1:5000) Western blots were as described (Calcagno-Pizarelli *et al.*, 2007; Galindo *et al.*, 2007; Hervás-Aguilar *et al.*, 2007). Constructs for integrative transformation (Supplementary Table 2) were confirmed by sequencing and were targeted to the *pyroA* or *argB* locus using published methodology (Calcagno-Pizarelli *et al.*, 2007; Pantazopoulou and Peñalva, 2009). Single copy integration was verified by Southern blots. AnVps8, AnVps45, AnVps34 (*pkiA*), AnVps19 (*vacA*), and *gdiA* were identified as AN0244, AN6531, AN4709, AN3144, and AN5895, respectively, in the *A. nidulans* genomic databases. Deletion cassettes were constructed by PCR (Szewczyk *et al.*, 2006; Supplementary Table 3), using $pyrG^{Af}$ (*AnVps45*Δ and *AnVps8*Δ) or $pyroA^{Af}$ (*rabB*Δ) as selection marker. Recipient strains carried *nkuA*Δ impairing nonhomologous recombination (Nayak *et al.*, 2005).

Microscopy

Cells were cultured at 25° on "watch minimal medium" (Peñalva, 2005) using Lab-Tek chambers (Nalge Nunc International, Rochester, NY); Pantazopoulou and Peñalva, 2009). Expression levels of fluorescent reporters under the control of $alcA^{p}$ were modulated by the carbon source (Abenza *et al.*, 2009): low levels were attained with 0.1% (wt/vol) fructose, and high-levels were obtained using 1% (vol/vol) ethanol or by preculturing cells on 0.02–0.05% (wt/vol) glucose and shifting them to 1% (vol/vol) ethanol for 3–4 h. 7-amino-4-chloromethylcoumarin (CMAC) vacuolar staining and ammonium-induced endocytic down-regulation of AgtA-GFP have been described (Abenza *et al.*, 2009; Pantazopoulou and Peñalva, 2009). Aggregation of EEs was induced with benomyl (4.8 μg/ml). Imaging of monomeric red fluorescent protein (mRFP)-RabB and GFP-RabA was started at 10 min after drug addition, after confirming, using time-lapse microscopy, that EE movement was fully arrested. Images were acquired with a Hamamatsu ORCA ER-II camera (Bridgewater, NJ) and a Leica DMI6000B microscope (Deerfield, IL) with an EL6000 external light source for epifluorescence excitation and HCX 63× 1.4 NA or 100× 1.4 NA objectives and Semrock Brightline GFP-3035B and TXRED-4040B (mRFP) filter sets. Strictly simultaneous imaging of GFP and mRFP channels was carried out with a Dual-View imaging system (Photometrics, Tucson, AZ), using the recommended filter sets (Pantazopoulou and Peñalva, 2009). Kymographs, contrast adjustment, color combining, Dual-View channel overlap (Photometrics), and z-stack maximal intensity projections (contrasted, when indicated, with the "sharpening" algorithm) were made using Metamorph (Molecular Devices, Sunnyvale, CA). Images were converted to 8-bit grayscale (and usually shown in inverted contrast) or to 24-bit RGB, and annotated with Corel Draw (Corel, Ottawa, Canada). Time-lapse sequences were converted to QuickTime using ImageJ 1.37 (http://rsb.info.nih.gov/ij/). When indicated, images were deconvolved using blind deconvolution (AutoDeblur software, Media Cybernetics, Bethesda, MD). Statistical analyses were performed using GraphPad Prism 5.00 for Windows (GraphPad Software, La Jolla, CA).

Pulldown Assays

We used a modification of a previous procedure (Rodríguez-Galán *et al.*, 2009). Glutathione *S*-transferase (GST) fusion proteins were expressed in *Escherichia coli* JM109-pRIL cells for 24 h at 18°C after induction with 0.1 mM isopropyl β-D-1-thiogalactopyranoside (IPTG). Bacterial pellets (100-ml cultures) were resuspended in (10 ml each) bacterial lysis buffer (BLB: PBS, pH 7.4, 1% Triton X-100) containing Roche's complete EDTA-free protease inhibitor cocktail (1 tablet in 50 ml of BLB) and lysed with a French Press. Lysates were cleared after centrifugation at 30,000 × *g* and 4°C for 30 min. Supernatants were incubated with 0.2 ml of 50% (vol/vol) glutathione-Sepharose 4B beads (Amersham, Piscataway, NJ), equilibrated in BLB, for 1 h at 4°C. Beads were washed three times with BLB (10 volumes each) and one additional time with binding buffer (BB: 20 mM Tris-HCl, 110 mM KCl, 5 mM $MgCl_2$ and 1 mM DTT, pH 8) before resuspension in BB (~50% vol/vol of slurry). The concentration of GST-Rabs obtained was ~10 μg/ml bead suspension. For loading with GDP and GTPγS, GST-Rab beads were washed once and resuspended in 1 ml of BB-*GTPγS* (BB containing 10 mM EDTA and 50 μM GTPγS (Jena Bioscience, Jena, Germany; NU-412–10) or BB-*GDP* (BB containing 10 mM EDTA and 50 mM GDP; Sigma, St. Louis, MO) before incubating for 30 min in a rotating wheel at 25°C. This procedure was repeated using BB-*GTPγS* or BB-*GDP* without EDTA.

To prepare prey protein extracts for pulldowns, strains carrying gene-replaced alleles expressing AnVps34, AnVps19, AnVps45, AnVps8, and GdiA, tagged at their C-termini with hemagglutinin (HA)3, were cultured in pH 6.5 (neutral) MFA (Hervás-Aguilar *et al.*, 2007). Mycelial biomass (0.5 g), collected by filtration and lyophilized, was distributed into five 2-ml tubes, ground to a fine powder using a FastPrep (4-mm ceramic bead; 10 s, power setting 4), and reconstituted with 1 ml/tube of *Aspergillus* binding buffer ABB [20 mM Tris-HCl, 110 mM KCl, 5 mM $MgCl_2$, 1 mM DTT, 10% (vol/vol] glycerol, 0,1% [vol/vol] Triton X-100, pH 8) containing 2.5 μM Pefabloc, 2 μM pepstatin, 1.2 μM leupeptin, and 2 μM MG132. The resulting suspension was mixed with one volume of glass beads (0.4–0.6 mm), and proteins were extracted with two FastPrep pulses (10 s each; power setting 4) followed by a 15-min incubation at 4°C in a rotating wheel. Extracts were clarified at 16,000 × *g* for 30 min at 4°C. Pooled supernatants (5 ml) were dialyzed against ABB to remove endogenous nucleotides and clarified by centrifugation at 16,000 × *g* for 30 min at 4°C before use.

For pulldowns, 20-μl aliquots of GTPγS- or GDP-loaded GST-Rab beads were mixed (Handee columns, Pierce, Rockford, IL; total volume, 800 μl) with 2 mg of *A. nidulans* protein extracts in ABB containing 0.5 mM GTPγS or GDP, as appropriate. Columns were incubated for 2 h at 4°C in a rotating wheel before washing the beads three times with 1 ml of 20 mM Tris-HCl, 175 mM KCl, 5 mM $MgCl_2$, 1 mM DTT, and 0.1% (vol/vol) Triton X-100, pH 8, containing 50 μM GTPγS or 50 μM GDP, as required. (Beads were incubated for 15 min at 4°C in a rotating wheel for the last two washes). Bound proteins were eluted after resuspension in 50 μl of Laemmli sample buffer. Twenty-microliter aliquots were resolved in 10% SDS-polyacrylamide gels that were transferred to nitrocellulose for anti-HA Western blotting. Western blots were reacted with Roche's anti-HA rat mAb (1/1000) and developed with Southern Biotechnology (Birmingham, AL) peroxidase-coupled goat anti-rat IgM+IgG secondary antiserum (1:4000) and Amersham Biosciences ECL. Five-microliter aliquots of the same samples were run in parallel SDS-polyacrylamide gels for Coomassie staining.

Affinity Purification of RabA and RabB Effectors

The methodology described below is an adaptation to *A. nidulans* of published procedures (Christoforidis and Zerial, 2000; Siniossoglou, 2005). GST-RabA and GST-RabB fusion proteins (0.8-l bacterial cultures) were immobilized onto 0.8 ml of 50% (vol/vol) glutathione-Sepharose 4B beads. Washed beads were divided into equal portions that were loaded at 30°C with GTPγS and GDP, respectively, using 1.5 ml of 50 μM GTPγS- or GDP-containing buffers. Lyophilized mycelia (2–14 g) were ground in liquid nitrogen with glass beads (0.4–0.6 mm) using mortar and pestle. The powder was resuspended in ABB (15 ml/g of lyophilized weight) containing 2.5 μM Pefabloc, 2 μM pepstatin, 1.2 μM leupeptin, and 2 μM MG132 and homogenized with three 30-s pulses (with 60-s intervening periods on ice) of a Braun MSK mechanical disintegrator (Neuhausen, Germany). Beads and large debris were removed after centrifugation for 30 min at 30,000 × *g* and 4°C. The supernatant (~120 ml) was filtered through two layers of Miracloth (Calbiochem, San Diego, CA), and remaining insoluble materials were pelleted for 70 min at 100,000 × *g* and 4°C before dialysis against two 6.5 l changes of ABB.

Dialyzed extracts were clarified by centrifugation at 100,000 × *g* and 4°C for 70 min and filtered through a 0.45-μm pore membrane. This procedure yielded ~100 ml of 12–15 mg/ml protein extract. Fifty-milliliter aliquots were mixed with 0.4 ml of 50% (vol/vol) glutathione-Sepharose beads containing the relevant GTPγS- or GDP-loaded GST-Rab. GTPγS or GDP (final concentration, 125 μM) was added to each mixture as appropriate, the mixtures were rotated for 2 h at 4°C and finally loaded onto plastic columns (Bio-Rad, Richmond, CA) that were allowed to drain, closed, and incubated for 10 min with of 3 ml of ABB containing 50 μM GTPγS or 50 mM GDP. The columns were then washed with 3 ml/column of buffer I (20 mM Tris-HCl, 220 mM KCl, 5 mM $MgCl_2$, and 1 mM DTT, pH 8; containing 50 μM GTPγS or 50 mM GDP) and with 1 ml/column of the same buffer without nucleotide. Bound material was eluted after incubation for 15 min at room temperature (RT) with 0.4 ml of elution buffer (20 mM Tris-HCl, 1.5 M KCl, 20 mM EDTA, 1 mM DTT, pH 8) containing either 5 mM GDP (proteins bound to the GTPγS-loaded GST-Rab) or 1 mM GTPγS (proteins bound to the GDP-loaded GST-Rab). Eluates were diluted with water, TCA-precipitated, and resuspended in 20 μl of Laemmli sample buffer. Aliquots were run in 10% SDS-polyacrylamide gels that were silver-stained for analytical purposes or stained with SYPRO-Rubi for protein isolation and subsequent mass spectrometry.

MALDI Peptide Mass Fingerprinting, Tandem Mass Spectrometry (MS/MS)MS/MS Analysis, and Database Searching

Proteins bands were excised manually from Sypro-stained gels and processed automatically in a Proteineer DP (Bruker Daltonics, Bremen, Germany), as

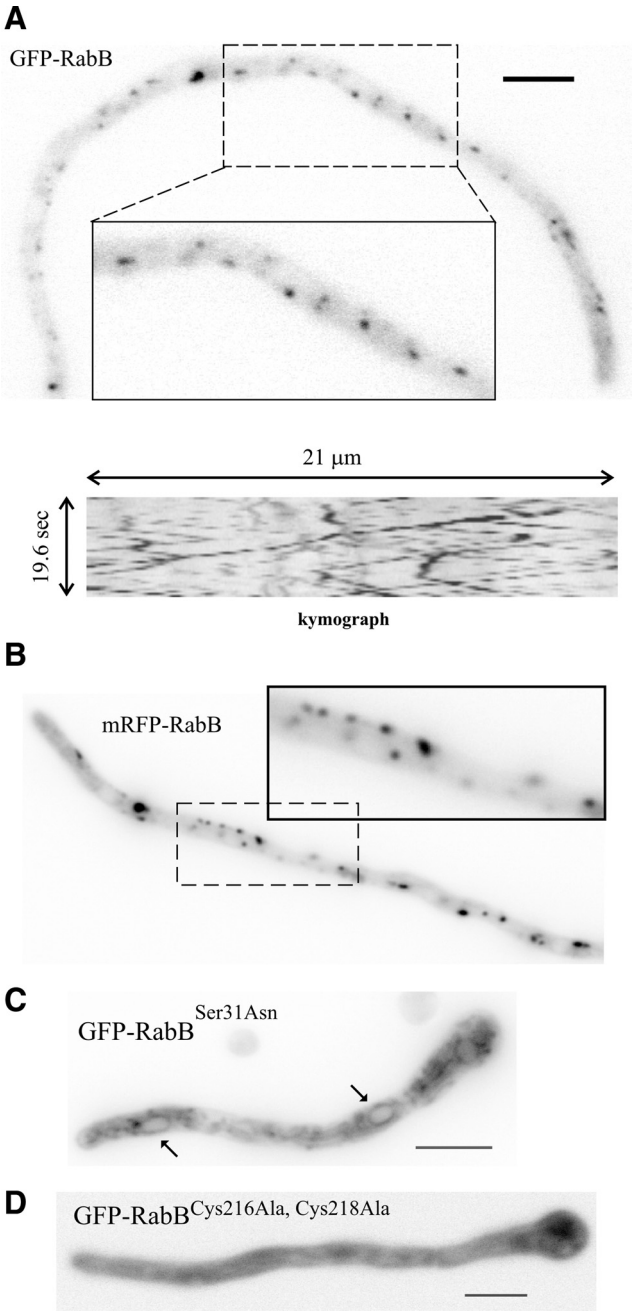

Figure 1. RabB localizes to motile punctate cytosolic structures. (A) Epifluorescence image of GFP-RabB corresponding to a still frame of Supplementary Movie 1. The kymograph illustrating the bidirectional motility of early endosomes corresponds to a 21-μm-long, 18-pixel-wide line covering the whole width of the hypha. (B) Epifluorescence image of mRFP-RabB (Supplementary Movie 2). (C) GDP-locked GFP-RabB^{Ser31Asn} mutant localizes to the cytosol and to faintly labeled reticulate structures corresponding to ER. Two nuclei are indicated with arrows. (D) Mutant GFP-RabB carrying Ala substitutions of C-terminal Cys residues (Cys216 and Cys218) that undergo geranylgeranylation is strictly cytosolic. Expression of GFP-tagged mutant and wild-type RabBs was driven by the *alcA*^{p}. Bar, 5 μm.

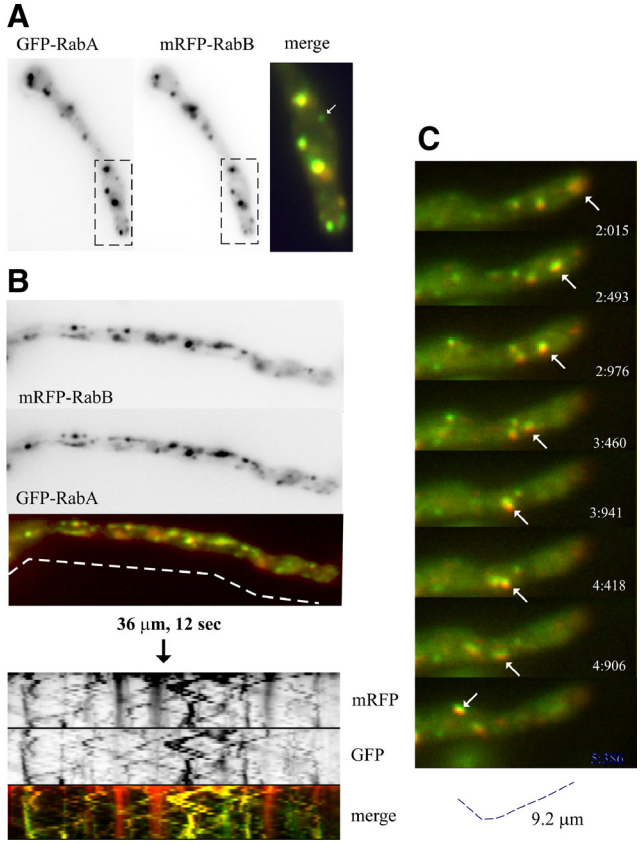

Figure 2. RabB and RabA colocalize on endosomes. (A) Red and green channels of a cell coexpressing mRFP-RabB and GFP-RabA that had been treated with benomyl, which prevents EE movement and leads to aggregation of EEs. The arrow in the magnified "merge" box indicates one rare example of a structure containing undetectable levels of RabB. (B) Dual-View still frames corresponding to Supplementary Movie 3. The merge of GFP and mRFP channels is shown. The kymographs below, corresponding to the dotted line, illustrate the essentially complete colocalization of RabA and RabB in motile endosomes. Note that a minor proportion of mRFP-RabB, seen after contrasting the images for color merge, is sorted to the vacuoles. Faintly labeled red vacuoles are seen in kymographs as fuzzy vertical bars, contrasting with strongly labeled, static mature endosomes. (C) Frames of a time-lapse sequence showing an arrowed endosome that contains RabA and RabB, moving retrogradely at ~3 μm/s.

described (Shevchenko *et al.*, 2006). Plugs were sequentially washed with 50 mM ammonium bicarbonate and acetonitrile before reduction with 10 mM DTT in 25 mM ammonium bicarbonate solution and alkylation with 55 mM iodoacetamide (Sigma) in 50 mM ammonium bicarbonate. Gel pieces were rinsed with 50 mM ammonium bicarbonate and acetonitrile before drying under nitrogen. Samples were digested with 16 ng/μl modified porcine trypsin (sequencing grade; Promega, Madison WI) in 25% acetonitrile/50 mM ammonium bicarbonate solution for 6 h at 37°C, and the resulting peptides were eluted with 0.5% TFA, transferred by centrifugation to V-bottomed 96-well polypropylene microplates, dried in a speed-vac, and resuspended in 4 μl of MALDI (matrix-assisted laser desorption/ionization) solution. Aliquots, 0.8 μl, were deposited onto a 389-well OptiTOF Plate (Applied Biosystems, Framingham, MA) and allowed to dry before addition of 0.8 μl of 3 mg/ml α-cyano-4-hydroxycinnamic acid (Bruker Daltonics) in MALDI solution, and were again allowed to dry.

For MALDI-TOF (time-of-flight) analysis, samples were analyzed in an ABI 4800 MALDI TOF/TOF mass spectrometer (Applied Biosystems, Framingham, MA, USA) in positive ion reflector mode; ion acceleration voltage was set to 25 kV for mass spectrometry (MS) acquisition and 1 kV for tandem mass spectrometry (MS/MS). Spectra were stored into the ABI4000 Series Explorer Spot Set Manager. Peptide map fingerprinting (PMF) and MS/MS fragmentation spectra were smoothed and corrected to zero baseline. Each PMF spectrum was internally calibrated with the mass signals of trypsin autolysis ions to reach a typical accuracy of <25 ppm. Known trypsin and keratin mass signals, as well as potential sodium and potassium adducts (+21.98 and +37.95 Da, respectively) were removed from the peak list. GPS Explorer v4.9 was used to submit the combined PMF and MS/MS data to Mascot software v.2.1 (Matrix Science, London, United Kingdom). Searches were conducted using the nonredundant National Center for Biotechnology Information (NCBI) and the *Aspergillus nidulans* databases. Search parameters were set as follows: enzyme, trypsin; fixed modifications, carbamidomethyl (C); allow up to one missed cleavage; peptide tolerance, 20 ppm; nd MS/MS tolerance, 0.5 Da. Protein scores >81 were considered significant ($p < 0.05$).

RESULTS

Previous work demonstrated that RabA localizes to EEs but is largely dispensable for the endocytic degradation of the plasma membrane transporter AgtA (Abenza *et al.*, 2009). This was unexpected, as sequence alignments suggested that RabA was closest to *S. cerevisiae* Vps21^{Ypt51}. We revisited this conclusion and noticed that RabA contains a long insertion of ~ 30 residues that is absent from human Rab5s and from RabB and that resembles in position, length, and amino acid sequence an insertion present in Ypt52p (Supplementary Figure 1). Thus, we concluded that RabB should be the *A. nidulans* Vps21p orthologue.

RabB Localizes to EEs

We established the subcellular localization of RabB using fluorescent fusion proteins. GFP- and mRFP-RabB, expressed under the control of the *alcA*^{p} promoter, phenotypically complement the null *rabB*Δ mutation (see below), indicating that they are functional (data not shown). We determined that both GFP-RabB and mRFP-RabB localize to punctate structures showing long-distance bidirectional motility (Figure 1A and B; for motility, see also Supplementary Movies 1 and 2). This motility is characteristic of EEs labeled with GFP-RabA (Abenza *et al.*, 2009; see also below), strongly suggesting that RabB structures are EEs.

For GFP-RabB we additionally demonstrated that this localization was independent of using the strong *alcA*^{p} or the *rabB*^{p} physiological promoter, showing that it does not result from an artifact due to overexpression. Moreover, a mutant RabB carrying a Ser31Asn substitution, predicted to lock RabB in the GDP conformation, mislocalizes to a cytosolic haze and to a faintly fluorescent network of endomembranes including the endoplasmic reticulum (ER; as indicated by the labeling of nuclear membranes; Figure 1C). Finally, mutant GFP-RabB in which prenylable Cys216 and Cys218 had been replaced by Ala residues is strictly cytosolic (Figure 1D). Thus, RabB appears to localize to EEs in a GTP switch- and prenylation-dependent manner.

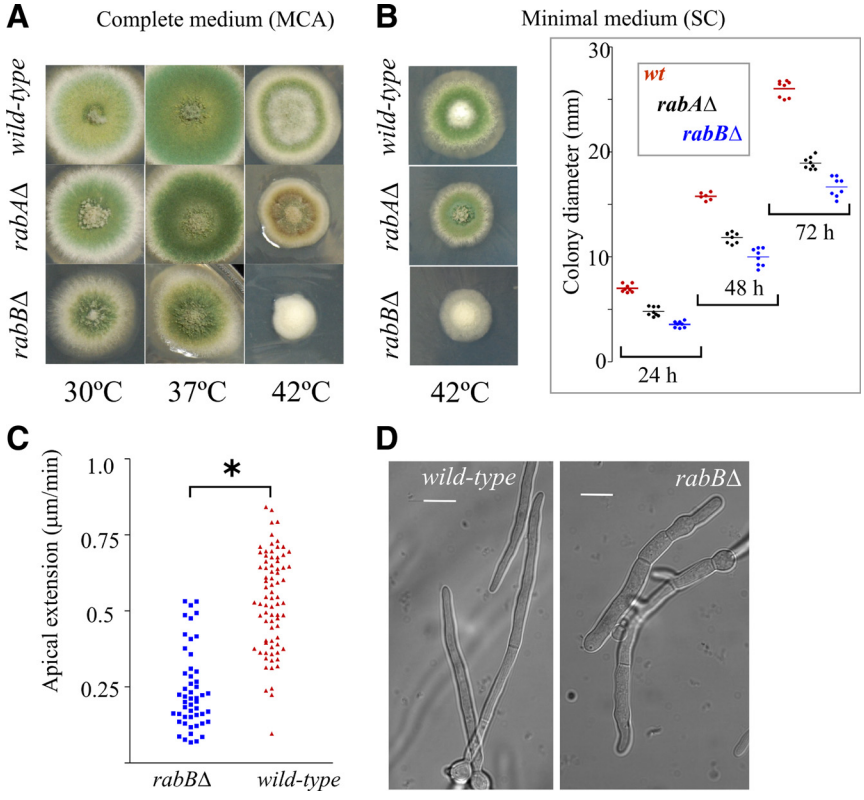

Figure 3. Growth phenotypes of null alleles of genes involved in early endosome function. (A) Strains were cultured on complete medium (MCA) plates that were incubated for 72 h at the indicated temperatures before being photographed. (B) Growth phenotype of the same strains on synthetic complete (SC) medium. Left, pictures were taken after a 72-h incubation at 42°C (for 37°C see also Figure 9G); right, radial colony growth of the indicated strains at 42°C. Diameters of colonies of the indicated genotypes were measured after 24, 48, and 72 h incubation at 42°C. Horizontal lines indicate average diameters (in mm) for each time point and genetic condition. Differences were statistically significant ($p < 0.001$) for all pair combinations. (C) Apical extension rate of wild-type ($n = 77$) and *rabB*Δ ($n = 51$) tips at 42°C. Differences are statistically significant; *$p < 0.001$, Student's *t* test. (D) Nomarski images of wild-type and *rabB*Δ cells cultured at 42°C.

RabA and RabB Cohabit on the Same Class of EEs

RabA motile structures are EEs, which are labeled with FM4-64 shortly after adding the membrane tracer (Abenza *et al.*, 2009). One possibility was that RabB localizes to this RabA-containing population of EEs. A second was that RabA and RabB localize to distinct EE populations. A third was that motile structures labeled with RabB do not actually represent EEs (for example, they could represent secretory membranes). To distinguish among these possibilities we used cells coexpressing GFP-RabA and mRFP-RabB. To circumvent the problem of the high motility of EEs, we first used the anti-MT drug benomyl, which abolishes movement, thereby leading to aggregation of RabA-containing EEs (Abenza *et al.*, 2009). RabB membranes colocalize with RabA in these aggregates (Figure 2A). Second, we recorded strictly simultaneous time-lapse series in the green and red channels using a Dual-View system (Photometrics). Analysis of time-lapse sequences and kymographs established that RabA and RabB colocalize in motile structures and therefore that RabA and RabB coexist on the same population of motile EEs (Figure 2, B and C; Supplementary Movie 3). RabA and RabB also colocalize in relatively static endosomes (vertical lines in Figure 2B kymographs) that are usually larger than motile EEs and that plausibly represent a late stage in endosome maturation that takes place with concomitant loss of motility.

RabB Is Important for Growth at High Temperatures

To determine the role of *rabB* in these EEs, we constructed a complete deletion by gene replacement. *rabB*Δ strains are viable. On complete medium, *rabB*Δ slightly impairs growth at 30° or 37°C (*A. nidulans* grows optimally at 37°C) and markedly impairs growth and conidiation at 42°C (Figure 3A). *rabA*Δ also impairs growth and conidiation at 42°C as reported (Abenza *et al.*, 2009), but its effects are much less conspicuous than those of *rabB*Δ (Figure 3A) On synthetic minimal medium plates, *rabB*Δ and *rabA*Δ strains show colony growth defects at 42°C (Figure 3B), but that of *rabB*Δ is reproducibly more pronounced (Figure 3B, right). As on complete medium, *rabB*Δ additionally prevents conidiation at 42°C (Figure 3B). These data strongly indicate that *rabB* plays a more important physiological role.

In agreement with radial growth tests, the mean apical extension rate of wild-type tips in synthetic complete liquid cultures at 42°C doubles that of *rabB*Δ tips (0.53 ± 0.018 vs. 0.21 ± 0.018 μm/min; Figure 3C). Microscopic observations also showed that, at 42°C, *rabB*Δ germ tubes are unusually wide (Figure 3D, compare with the wild type).

rabBΔ *Leads to a Class B-like Vacuolar Phenotype*

CMAC staining of vacuoles revealed that *rabB*Δ strains contain atypically small vacuoles (Figure 4). In the wild type, where the size of the vacuoles decreases with the distance to the tip (Peñalva, 2005), the basal conidiospore usually contains a single large vacuole (Figure 4A). Thus, the reduction in vacuolar size seen in the mutant is most noticeable in conidiospores, where *rabB*Δ strains contain several small vacuoles (Figure 4A). We measured the diameters of vacuoles in a sample of 17 germlings (Figure 4B). Vacuoles were 2.75 times smaller on average in the mutant than in the wild type when only those located within the conidiospore were considered (Figure 4B, left) and ~ 1.5 times smaller ($p < 0.0001$) when vacuoles located within the more basal 10 μm of the germ tube were measured (Figure 4B). (In more apical regions, the small differences observed were not statistically significant). The finding *rabB*Δ results in smaller vacuoles

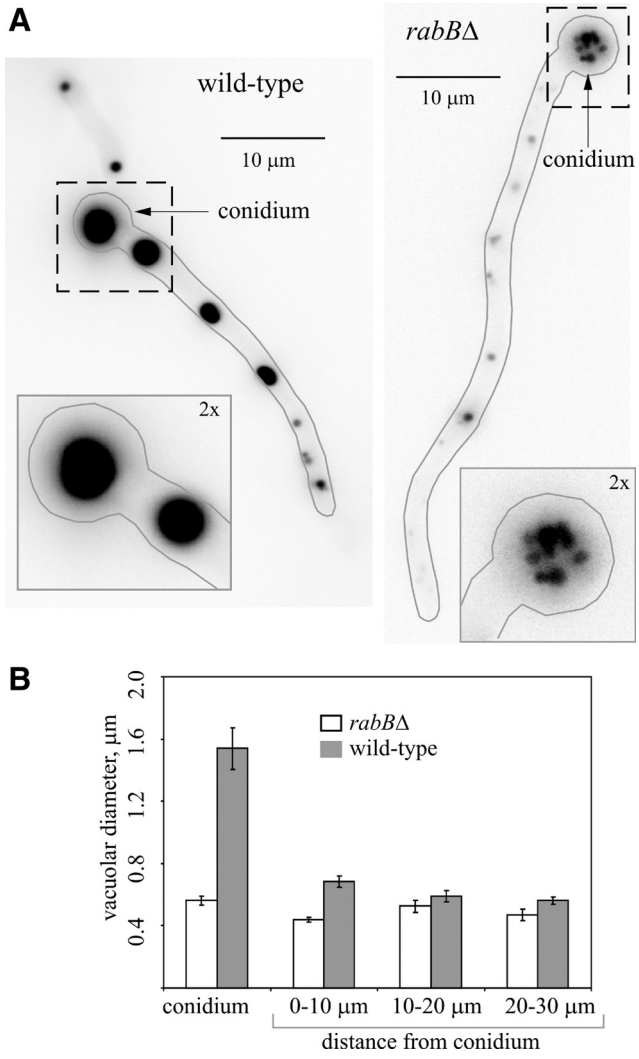

Figure 4. *rabB*Δ results in vacuolar fragmentation. (A) Conidiospores of wild-type and *rabB*Δ strains were germinated at 25°C. The resulting germlings were stained with CMAC, which labels the lumen of vacuoles, and photographed by epifluorescence microscopy using a Leica D filter set. The contours of the germlings are indicated with gray lines. Insets, close-up (2× magnifications of the large fields) of the regions (dotted squares) corresponding to the basal conidiospores (conidium, indicated with arrows). (B) Quantification of vacuolar size. Germlings of similar length were segmented into four different regions. One was the basal conidiospore, and the three other were 10-μm-long regions increasingly distant from the basal conidiospore, as indicated. The average vacuolar diameter for each region was measured. Error bars, SE.

was unexpected, because in *S. cerevisiae vps21*Δ results in enlarged rather than smaller vacuoles (Horazdovsky *et al.*, 1994). In contrast, in work to be reported elsewhere we showed that deletion of the *A. nidulans YPT7* homologue (also denoted *avaA*; Ohsumi *et al.*, 2002) results in vacuolar fragmentation, as in *S. cerevisiae*. Thus, the vacuolar phenotype of *rabB*Δ strongly suggests that the deletion impairs vacuolar biogenesis.

Long-Distance Movement of EEs Is Specifically Dependent on RabB

FM4-64 uptake experiments (Peñalva, 2005) showed normal internalization in the *rabB*Δ mutant, such that at the 45–60-

min final time points the dye labeled the rim of the vacuoles and the mitochondrial/ER membranes, as in the wild type. However, time-lapse sequences taken at early time points (2–10 min) revealed that *rabB*Δ prevents the motility of EEs: In the wild type, 58.8% of n = 536 EEs were characteristically motile (of these, about half moved basipetally and half acropetally). In sharp contrast, only 10.4% of n = 549 *rabB*Δ EEs showed anterograde or retrograde motility (Figure 5A; Supplementary Movies 4 and 5; this nearly sixfold reduction in motility was seen for both basipetally and acropetally moving endosomes). Kymographs (Figure 5A, below the corresponding hyphae) clearly illustrate the loss of motility of FM4-64 EEs. As even at early time points FM4-64 reaches immotile LEs, we repeated these experiments using GFP-RabA and GFP-RabB as more specific EE reporters. Loss of EE motility resulting from *rabB*Δ was clearly seen by comparing GFP-RabA time-lapse movies and kymographs from *rabB*Δ and *rabB*$^+$ strains (Figure 5B; Supplementary Movies 6 and 7). However, *rabA*Δ did not prevent movement of EEs labeled with GFP-RabB (Figure 5B; Supplementary Movies 8 and 9), showing that RabB is crucially required for EE motility.

AnVps34 and AnVps19 Are RabB, But Not RabA, Effectors

Rab5 recruits human Vps34 phosphatidylinositol-3-kinase (PI3K) to endosomal membranes through interaction with its regulatory subunit p150 (Christoforidis *et al.*, 1999b). In *S. cerevisiae*, it is well established that PI(3)P cooperates with Vps21p in the endosomal recruitment of Vps19p (also denoted Vac1p in yeast), which in turn recruits Vps45p (Peterson *et al.*, 1999; Tall *et al.*, 1999). However, whether GTP-Vps21p

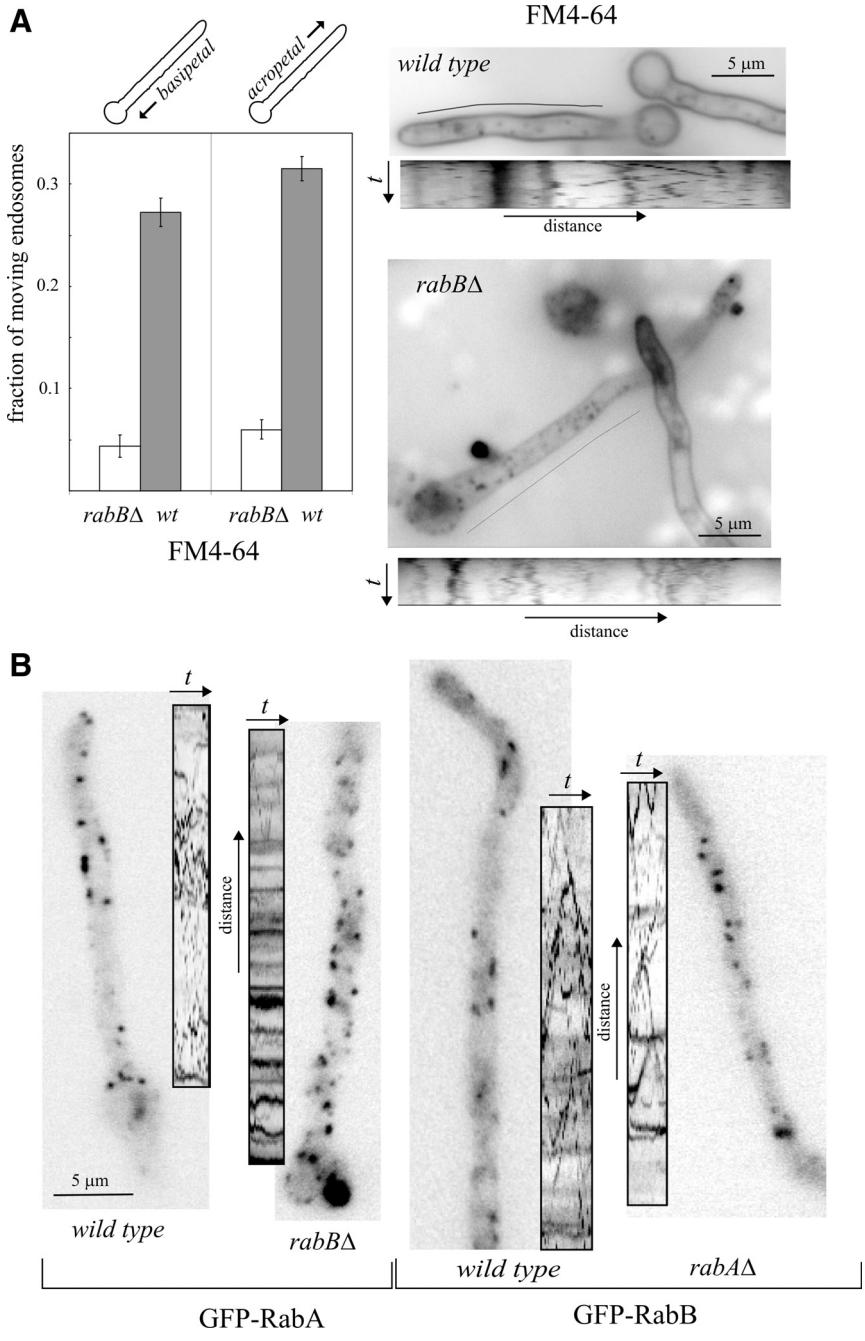

Figure 5. *rabB*, but not *rabA*, is required for early endosome motility. (A) Cells were imaged within 5–10 min after FM4-64 loading to label endosomes. In the wild-type, generally smaller early endosomes are motile, whereas larger endosomes are static. *rabB*Δ reduced the proportion of endosomes moving in either basipetal or acropetal direction nearly six times. This marked reduction is illustrated by the kymographs on the right (time dimension, 15 s), corresponding to Supplementary Movies 4 (wild-type) and 5 (*rabB*Δ). For unknown reasons, FM4-64 appears to be either less fluorescent or more susceptible to photobleaching in the plasma membrane of the mutant than in the wild-type. Note that because FM4-64 labels both early and late endosomes, the proportion of static structures is higher than that seen when early endosome-specific GFP-RabA or GFP-RabB are used as reporters. (B) GFP-RabA and GFP-RabB EEs visualized in wild-type and mutant germlings, all shown at the same magnification (size bar in left image). In this panel, kymographs correspond to 10–13 s Movies (Supplementary Movies 6 through 9) and are shown at the same scale as the corresponding still image.

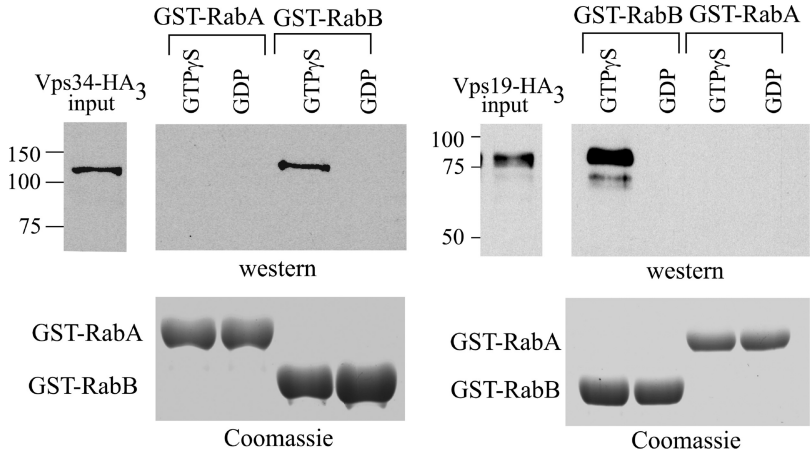

Figure 6. AnVps19 and AnVps34 are RabB, but not RabA, effectors. GST pulldown assays with the indicated GST-Rab protein baits. Extracts from cells expressing AnVps19-(HA)3 (in *S. cerevisiae* Vps19p is also known as Vac1p) and AnVps34-(HA)3 at physiological levels were incubated with GST-RabA or GST-RabB glutathione-Sepharose beads, loaded with GTPγS or GDP. The proteins copurifying with the baits were analyzed by anti-HA Western blots. Input lanes contain 5% of the total material used for pulldowns.

recruits Vps34p PI3K to endosomes remains to be established. To gain insight into the roles of RabA and RabB, we tagged the C-termini of AnVps19, AnVps45 (see below), and AnVps34 with (HA)3 by gene replacement and used cell extracts expressing these proteins in pulldown assays with GST-Rab baits loaded with GDP or GTPγS. These experiments demonstrated that AnVps34 is pulled down by GTP-RabB but not by GDP-RabB, GDP- or GTP-RabA (Figure 6) and GDP- or GTP-AnRabE^{Ypt31} (data not shown; RabE^{Ypt31} is predicted to play roles in the late Golgi). Thus, *A. nidulans* Vps34 is a RabB effector. Moreover, also AnVps19 [itself a PI(3)P effector] specifically copurified with RabB-GTP but not with GDP-RabB and GDP- or GTP-RabA (Figure 6). Additional control experiments showed that AnVps34 and AnVps19 are not unspecifically bound by GST either (Supplementary Figure 2), and data described below provide evidence that GST-RabA, although unable to bind these RabB effectors, is able to undergo the conformational shift. Therefore, a major conclusion of these experiments is that RabB but not RabA should play a major role in determining degradative endosome membrane identity (i.e., EEs that will mature into late endosomes and, ultimately, undergo fusion with vacuoles).

Endosomal PI(3)P Is Dependent on RabB In Vivo

To corroborate that RabB is a major determinant of PI(3)P synthesis on endosomes, we determined the subcellular localization of PI(3)P-containing membranes in vivo using a fluorescent protein probe consisting of a duplicated FYVE domain of the *A. nidulans* ESCRT-0 protein Vps27/Hrs1 fused to GFP (Figure 7). In the wild type, (FYVE^{Vps27})$_2$::GFP localized to small and large punctae. Small punctae were more abundant and showed the characteristic bidirectional motility of EEs (Figure 7C, kymograph; readers should consult Supplementary Movie 10). Large punctae were relatively static and frequently associated with vacuoles, whose membranes were faintly labeled by the reporter (Figure 7B). In sharp contrast, (FYVE^{Vps27})$_2$::GFP predominated in the cytosol of *rabB*Δ cells, where motile EEs and large punctae were virtually absent and only a few faintly stained static structures were eventually seen (Figure 7D). In addition, the reporter labeled vacuolar membranes. (FYVE^{Vps27})$_2$::GFP-decorated vacuoles were more conspicuous near the basal conidiospore (Figure 7E). These findings agree with the prediction that PI(3)P is synthesized in EEs that eventually mature into late endosomes and led us to conclude that RabB is the major determinant of AnVps34 recruitment to endosomes. However, the fact that *rabB*Δ does not preclude (FYVE^{Vps27})$_2$::GFP localization to vacuoles suggests that the vacuolar PI(3)P pool cannot be solely originated from the endosomal pool, in agreement with published work (Kihara *et al.*, 2001). (This could not be tested directly because Vps34 is virtually essential in *A. nidulans*; A.P. and M.A.P., unpublished results). As expected from the inability of RabA-GTP to pull down Vps34, *rabA*Δ does not prevent (FYVE^{Vps27})$_2$::GFP localization to endosomes (Figure 7F; nor does it prevent the vacuolar localization; data not shown).

rabBΔ *Cells Missort Endocytic Cargo Destined to the Vacuolar Lumen*

PI(3)P in endosomal membranes recruits the ESCRT complexes mediating MVB sorting. Thus, PI(3)P depletion should prevent vacuolar degradation of endocytic cargo. We tested this prediction using the GFP-tagged glutamate permease AgtA, a prototypic example of a plasma membrane transporter down-regulated by endocytosis. In the wild type cultured on glutamate, AgtA-GFP is present in vacuoles but predominates in the plasma membrane (Figure 8A, 0 min). On shifting cells to ammonium, *agtA* transcription is shut off, and the pool of permease at the plasma membrane is endocytosed and delivered to the vacuolar lumen (Apostolaki *et al.*, 2009; Figure 8A, NH_4^+). Western blots of membrane proteins showed that, as expected, vacuolar delivery correlates with a sharp reduction in levels of AgtA-GFP (Figure 8C) after 40–60 min of shifting wild-type cells to ammonium. A similar reduction in levels was observed using endogenously tagged AgtA-(HA)3, demonstrating that it occurs irrespective of the tag used (Figure 8D).

In *rabB*Δ cells cultured on glutamate the plasma membrane predominance of AgtA was more conspicuous, and the vacuolar localization was markedly less prominent than in the wild type (Figure 8B, 0 min). Importantly, when *rabB*Δ cells were shifted to ammonium, AgtA-GFP did not reach the vacuolar lumen and instead localized to a cytosolic haze and to punctate, static cytosolic structures, clearly distinct from the vacuoles (Figure 8B, NH_4^+). This impairment in vacuolar delivery correlated with essentially abolished ammonia-dependent AgtA degradation as determined by Western blotting using AgtA-GFP (Figure 8C) or AgtA-(HA)3 (Figure 8D). As AgtA-GFP does not reach the vacuolar membranes either; *rabB*Δ prevents both the MVB sorting of AgtA and its traffic from endosomes to vacuoles.

As control, we used the endocytic recycling cargo SynA^{Snc1}-GFP (Valdez-Taubas and Pelham, 2003; Taheri-Talesh *et al.*, 2008). In the wild type, SynA-GFP is markedly polarized,

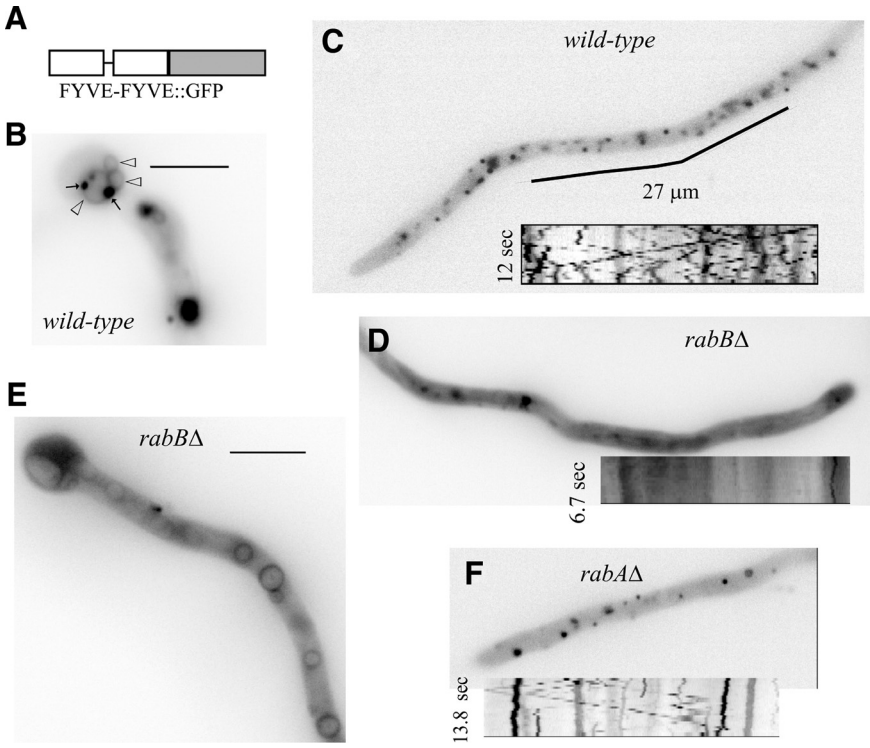

Figure 7. *rabB*Δ early endosomes are deficient in PI(3)P. (A) The PI(3)P reporter consists of a C-terminal fusion of GFP to two tandem copies of the AnVps27 FYVE domain. (B) $(FYVE^{Vps27})_2$::GFP labels faintly the membrane of basal vacuoles (open arrowheads), which frequently showed closely associated $(FYVE^{Vps27})_2$::GFP punctae (arrows). (C) Tip-proximal region of a wild-type hypha showing localization of $(FYVE^{Vps27})_2$::GFP to small punctae. The kymograph insert (Supplementary Movie 10) illustrates how a proportion of these punctae show the characteristic bidirectional motility of EEs. Relatively immotile ones represent, in all likelihood, late endosomes. (D and E) In *rabB*Δ cells $(FYVE^{Vps27})_2$::GFP localizes mainly to the cytosol and, in tip-distal regions, also to vacuolar membranes. The few punctae that were discernible against the cytosolic fluorescence haze were immotile (inserted kymograph). (F) *rabA*Δ cell showing the localization of $(FYVE^{Vps27})_2$::GFP to punctate structures, as in the wild type. Some punctate structures show characteristic EE motility (kymograph).

localizing to the apical dome. Polarization was essentially unaffected by *rabB*Δ, indicating that RabB does not play a major role in endocytic recycling (Figure 8E).

RabB and, to a Lesser Extent, RabA Can Recruit CORVET to Endosomal Membranes

Endosomal maturation into vacuoles or lysosomes occurs concomitant with the conversion of Rab5 domains into Rab7 domains. In *S. cerevisiae* such conversion involves the CORVET and the HOPS tethering complexes, acting at the endosomal and vacuolar levels, respectively (Sato *et al.*, 2000; Seals *et al.*, 2000; Peplowska *et al.*, 2007). We used affinity chromatography with GST-RabB and GST-RabA baits to identify, by mass spectrometry, those proteins that were retained by RabA and RabB in their GTP (i.e., loaded with GTPγS) but not in their GDP conformations (Figure 9, A and B). We determined, using filter binding assays (Supplementary Figure 3) that GST-RabA and GST-RabB did not show major differences in their ability to bind [γ-^{32}P]-GTP (Supplementary Figure 3). We also established that both RabB- and RabA-GDP affinity columns preferentially retained the *A. nidulans* GDP-dissociation inhibitor (AnGdiA), demonstrating that the baits had undergone the conformational switch in the presence of GTPγS (Figure 9, A and C; note that the gel corresponding to panel C was run under different conditions to improve the separation between GST-RabA and GdiA; efficient GdiA binding was also demonstrated by pulldown assays; see below).

Notably, RabB-GTP retained several prominent bands that MS/MS analyses showed to be the six components of CORVET (Figure 9A; Supplementary Table 4). The distinctive pattern of CORVET bands was also obtained with RabA-GTP (also confirmed by MS/MS; Supplementary Table 4), although RabA was notably less efficient (Figure 9B). Thus RabB and, to a lesser extent, RabA are able to recruit CORVET to endosomal membranes. To buttress this conclusion, we tagged with (HA)3 the chromosomal copy of the key CORVET subunit Vps8 (Markgraf *et al.*, 2009) and used extracts of cells expressing AnVps8-(HA)3 at physiological levels in pulldown assays. Both RabA-GTP and RabB-GTP pulled down AnVps8, but RabB was markedly more efficient (Figure 9E), roughly correlating with the efficiency of CORVET retention by the respective proteins in affinity columns. In contrast, GST-$RabN^{Ypt7}$, which is competent to recruit HOPS (our unpublished data) or GST alone are unable to recruit AnVps8 (Figure 9E; Supplementary Figure 2). As additional evidence that differences in the ability to recruit effectors do not result from inability of GST-RabA to undergo the conformational switch efficiently, we endogenously tagged GdiA with (HA)3 (GdiA corresponds to AN5895 in *A. nidulans* databases) and made pulldown experiments with the corresponding cells extracts (Figure 9D). These showed that GdiA-(HA)3 is efficiently bound both by GDP-RabA and by GDP-RabB, but not by their respective GTPγS-loaded forms or by GST treated with GDP or GTPγS (Figure 9D). Thus, we conclude that AnVps8/CORVET is more efficiently recruited by RabB than by RabA, indicating that RabB and, to a lesser extent, RabA are involved in the maturation of EEs into LEs.

AnVps45 Is a RabB, But Not a RabA, Effector

Notably, AnVps45 was efficiently eluted from RabB-GTP affinity columns (Figure 9A and Supplementary Table 4), whereas RabA-GTP columns were unable to bind this protein (Figure 9B), indicating that AnVps45 is a highly specific RabB effector. This conclusion was further confirmed by endogenously tagging the chromosomal copy of AnVps45 with (HA)3 and using extracts containing physiological levels of this protein in GST pulldown experiments. These confirmed that AnVps45 is efficiently pulled down by RabB-GTP but not at all by RabA-GTP or $RabE^{Ypt31}$-GTP, used as an additional specificity control (Figure 9F). We next deleted

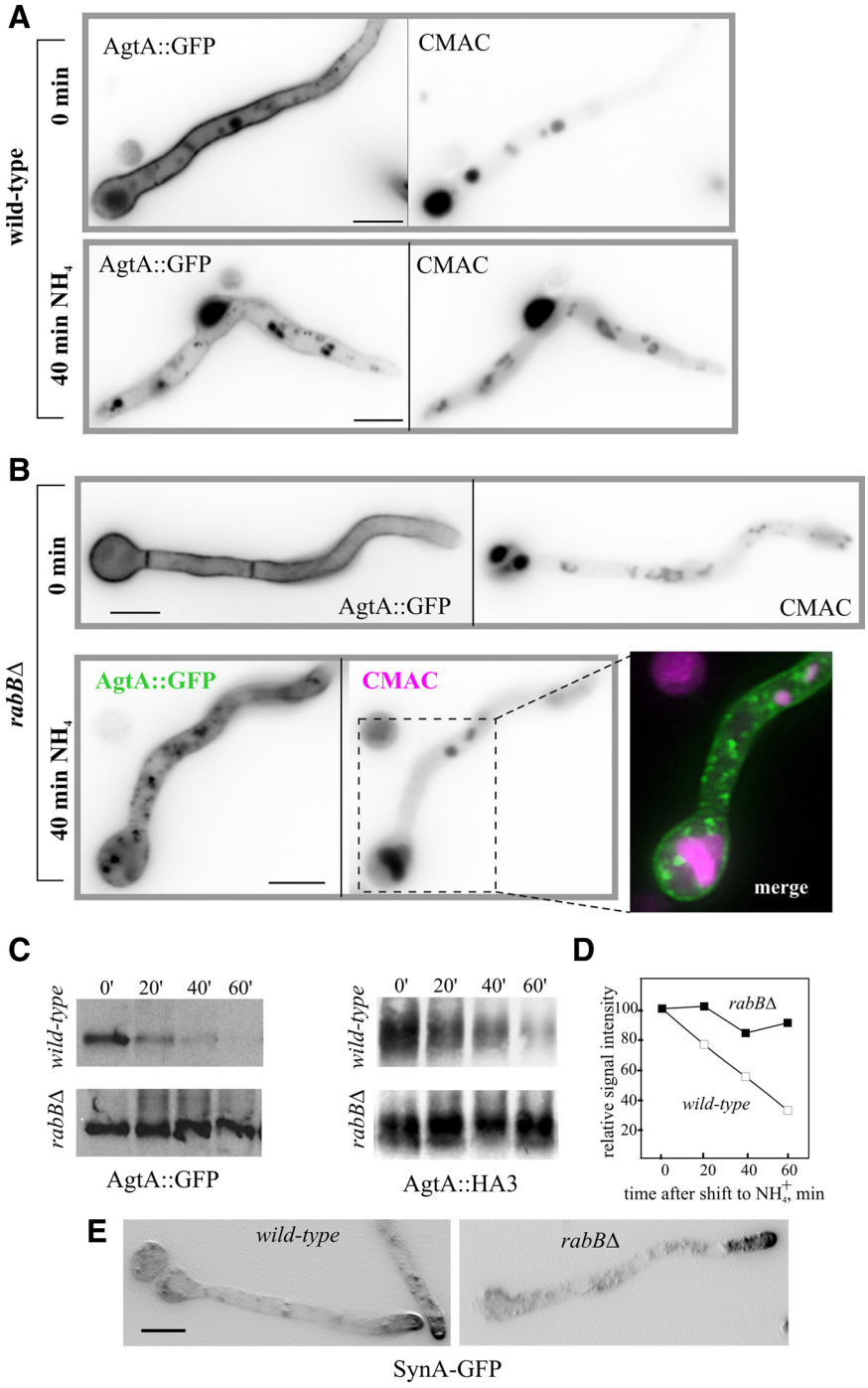

Figure 8. RabB is required for MVB sorting of the endocytic degradation cargo AgtA but not for the endocytic recycling of the SynA synaptobrevin homologue. (A) Wild-type cells expressing AgtA-GFP were cultured on 5 mM glutamate synthetic complete medium to induce the synthesis of the permease (0-min time point) and then shifted to the same medium containing 10 mM NH_4^+, which shuts off *agtA* transcription and promotes the endocytic down-regulation of the transporter. The positions of vacuoles were revealed with CMAC. (B) As above, using *rabB*Δ cells. Note the nearly complete localization of AgtA-GFP to the plasma membrane in glutamate-cultured cells (0 min). On shifting cells to ammonium, the permease is internalized to punctate cytosolic structures, which do not show any overlap with vacuoles stained with CMAC (merge; vacuoles shown in magenta; AgtA-GFP, green). Images are maximal intensity projections of z-stacks. (C) Western blot analyses of AgtA-GFP in cells cultured on glutamate (0 min) and shifted to ammonium for the indicated time points. The blot was reacted with anti-GFP antibody. (D) Western blot analyses of AgtA-(HA)3 cells cultured on glutamate (0 min) and shifted to ammonium for the indicated time points. The blot was reacted with anti-HA antibodies. The graph shows a quantitative analysis of AgtA-(HA)3 signals as a function of time. Approximately equal loading in the different lanes was confirmed by Ponceau staining of the nitrocellulose membrane (E) *rabB*Δ does not prevent the polarization of $SynA^{Snc1}$-GFP to the apical plasma membrane. Shown are maximal intensity projections of z-stacks contrasted with the "sharpen" function of Metamorph. Bars, (A, B, and E) 5 μm.

the gene encoding AnVps45. Albeit marginally viable, *Anvps45*Δ strains are severely debilitated, in sharp contrast with *rabB*Δ strains, which grow reasonably well (Figure 9G). This demonstrates that AnVps45 plays additional physiologically important functions that are RabB independent. These as yet unidentified functions cannot be RabA dependent either, as AnVps45 is not a RabA effector (Figure 9F).

RabB Becomes Essential in the Absence of RabA

The above data indicate that although RabB plays a unique role in establishing degradative endosome identity, RabA shows partially overlapping functions with RabB in the maturation of these endosomes. We demonstrated that *rabA*Δ and *rabB*Δ are synthetically lethal by two different methods. First, we set up a cross homozygous for *pyrG89* and *pyroA4* and heterozygous for *rabA*Δ*::pyrG*^{Af} and *rabB*Δ*::pyroA*^{Af} null mutations in repulsion, such that the double mutant recombinant progeny (*rabA*Δ*::pyrG*^{Af} *rabB*Δ*::pyroA*^{Af}), unlike the parental strains, should have been prototrophic. We obtained no such recombinants in a total of n = 112 progeny despite the fact that the reciprocal double auxotrophic class (*pyrG89 pyroA4 rabA*$^+$ *rabB*$^+$) was recovered at approximately the expected frequency (n = 32). We next plated on selective medium without pyridoxine and pyrimidines a number of viable progeny

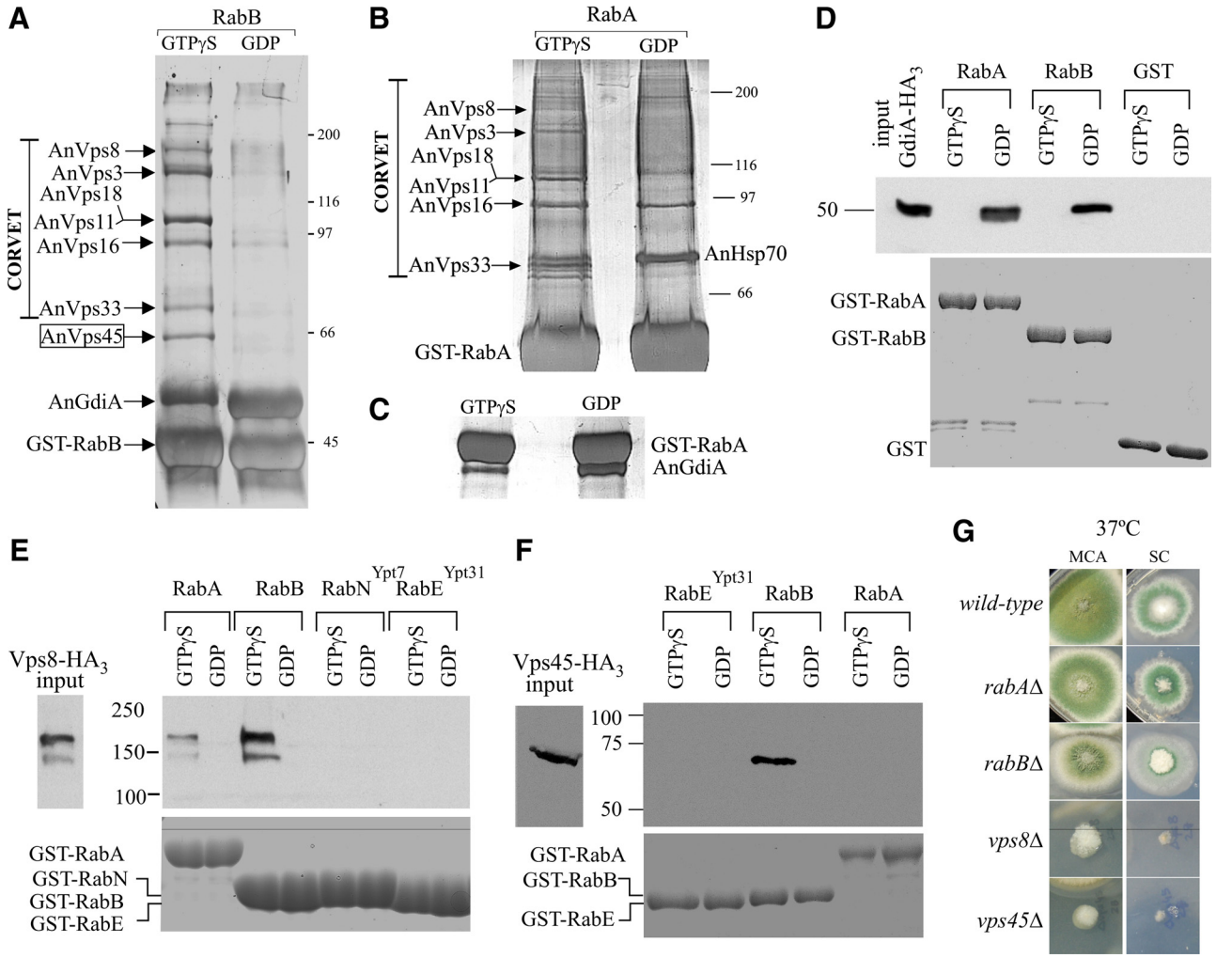

Figure 9. RabB and, to a lesser extent, RabA are able to recruit CORVET, but only RabB recruits AnVps45. (A) *A. nidulans* extracts were run through glutathione-Sepharose columns loaded with GTPγS- or GDP-RabB. Proteins retained by the columns were eluted and analyzed by SDS-PAGE and silver staining. The identity of the different bands was determined by MS of bands excised from preparative gels (Supplementary Table 4). (B) As in A but using GST-RabA–loaded affinity columns. (C) A region of an SDS-PAGE gel corresponding to the eluates of GTPγS- and GDP-RabA columns. The gel was run to allow resolution of the GST-RabA and GdiA bands. (D) Pulldown assays (as in Figure 6) of AnGdiA-(HA)3–containing cell extracts using the indicated protein baits. Input:,10% of the material used for the pulldown. (E) Pulldown assays of AnVps8-(HA)3–containing cell extracts using the indicated protein baits. Input, 5% of the material used for the pulldown. RabE is the *A. nidulans* orthologue of *S. cerevisiae* Ypt31p, and RabN the *A. nidulans* orthologue of *S. cerevisiae* Ypt7p. The faster mobility band detected with AnVps8-(HA)3 very likely results from partial proteolysis during protein extraction/incubation (AnVps8 is a large 177-kDa protein) (F) Pulldown assays of AnVps45-(HA)3, as above. (G) Strains of the indicated genotypes were cultured on complete (MCA) or synthetic complete (SC) medium.

sufficient to contain, assuming Mendelian segregation, 1375 double mutant recombinants and obtained none. However, inspection of these plates with a stereomicroscope revealed the presence of a number of submillimetric colonies that were unable to progress on the selective medium and that undoubtedly represent the double recombinant class (compare a "normal" colony obtained on nonselective medium with these microcolonies; Figure 10A). These data strongly indicated that the double mutant combination is very nearly lethal. To confirm this conclusion, we attempted to replace *rabA* by *pyrG*^{Af} in a *rabB*Δ*::pyroA*^{Af} *pyroA4 pyrG89* background by transformation. We obtained prototrophic primary transformants carrying double *rabA*Δ*::pyrG*^{Af} *rabB*Δ*::pyroA*^{Af} mutant nuclei in diploids/merodiploids and in heterokaryosis (Figure 10B). However, when individual nuclei of the heterokaryotic clones were segregated into conidiospores, we could only recover marginal growth in the absence of pyrimidines, indicative of severely impaired viability of the double mutant (Figure 10C). These data strongly suggest that RabA and RabB share a partially overlapping, essential function. Because both RabB and RabA recruit CORVET to endosomes, the simplest interpretation of this synthetic lethality is that such recruitment is essential in *Aspergillus*. Another possibility would be that RabA has some as yet unidentified function which becomes essential in the absence of RabB or vice versa. To distinguish between these possibilities, we deleted *AnVps8*, which was chosen because *S. cerevisiae* cells lacking Vps8p are unable to assemble CORVET (Peplowska *et al.*, 2007). Homokaryotic An*vps8::pyrG*^{Af} clones were severely debilitated but viable (Figure 9G), indicating that the CORVET function is very important but not absolutely essential for *A.*

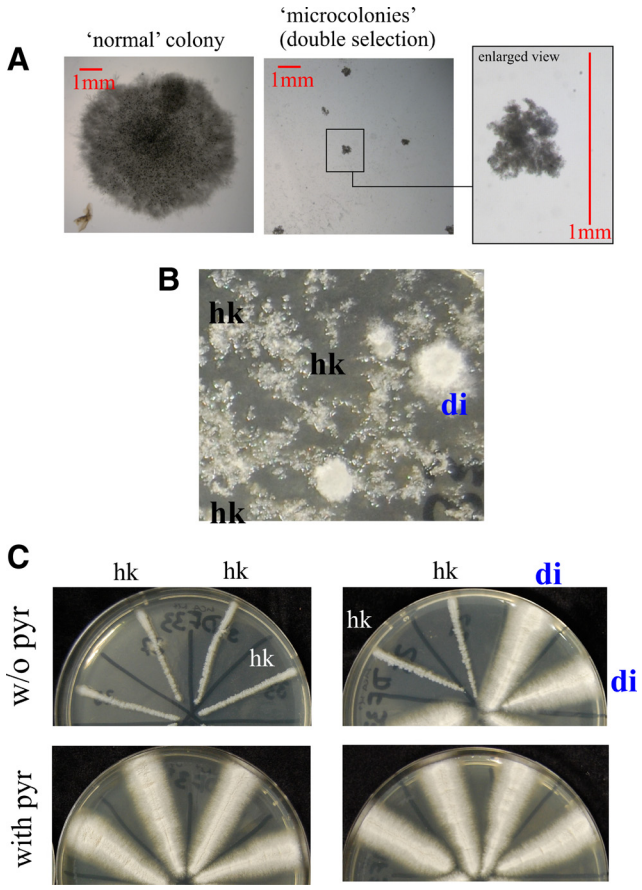

Figure 10. *rabB*Δ and *rabA*Δ are synthetically lethal. (A) Analysis of the progeny of a cross between parental strains with genotypes *rabA*Δ*::pyrG*^{Af} *pyroA4 pyrG89* (thus pyridoxine requiring) and *rabB*Δ*::pyroA*^{Af} *pyroA4 pyrG89* (thus pyrimidine requiring). Left, normal size colony arising from the progeny of this cross plated on synthetic complete medium (i.e., containing the nutritional supplements required by all parental and recombinant progeny genotypes). Middle and right, microcolonies of the progeny plated on double selective medium. Only *rabA*Δ*::pyrG*^{Af}, *rabB*Δ*::pyroA*^{Af} double mutants were expected to grow in the absence of both pyrimidines and pyridoxine. Note the minute size of the colonies (colonies in left and middle pictures are at the same magnification). The enlarged region shown on the right illustrates the submillimetric size of the colonies. (B) Protoplasts of the above *rabB*Δ*::pyroA*^{Af} *pyrG89 pyroA4* strain were transformed with a *rabA*Δ*::pyrG*^{Af} deletion cassette. Heterokaryotic, prototrophic clones (hk) were mostly recovered on minus-pyrimidine plates alongside with spontaneous diploid/merodiploids (di) arising during transformation. (C) Single nuclei segregate into conidiospores. Conidiospore transfers from heterokaryons gave rise to mycelium on pyrimidine-supplemented but not on pyrimidine-deficient MCA plates, indicating that, in the *rabB*Δ background, the *rabA*Δ*::pyrG*^{Af} deletion is lethal (single *rabA*Δ or *rabB*Δ mutants are viable on complete medium, Figure 3). In contrast, merodiploid/diploid strains (di) grew normally on both media.

nidulans. Consequently, the essentially lethal phenotype of the double *rabA*Δ *rabB*Δ mutation cannot be solely attributed to the inability to recruit CORVET to endosomes.

DISCUSSION

This and a previous article (Abenza *et al.*, 2009) represent a detailed functional analysis of the two *A. nidulans* Rab5 paralogues, RabA and RabB, which colocalize on endosomes. Unlike RabA, RabB mediates endosomal recruitment of the Vps34 PI3K, the PI(3)P-binding protein Vps19 and the SM protein Vps45, and thus it is functionally equivalent to *S. cerevisiae* Vps21p. As PI(3)P is a key determinant of degradative endosome identity, these findings indicated that RabB should play the major role in endocytic down-regulation, which was demonstrated using an endocytic cargo that undergoes vacuolar degradation. Whereas it is well established that fungal endosomes contain PI(3)P, this is the first demonstration that, like in mammalian cells (Christoforidis *et al.*, 1999b), the Vps34 PI3K is an effector of a fungal Rab5. We note that *A. nidulans* has an orthologue of yeast Vps15p/mammalian p150, an auxiliary subunit of the PI3K. We have not investigated the role of this protein (encoded by AN0576) in endosomal biogenesis or in the recruitment of AnVps34 by RabB.

This is also the first report, outside *S. cerevisiae*, that Rab5 (i.e., RabB and, to some extent, RabA) recruits CORVET. Thus, the mechanism proposed for late endosome/vacuole biogenesis in *S. cerevisiae* is almost certainly of general applicability: Rab5 recruits CORVET, which mediates the maturation of EEs into LEs. Once endosomes reach a certain stage of maturation, Rab5 domains undergo conversion into Rab7 (Ypt7) domains, and HOPS substitutes for CORVET to mediate homotypic vacuolar fusion (Subramanian *et al.*, 2004; Peplowska *et al.*, 2007; Markgraf *et al.*, 2009; Figure 11). Although RabB coordinates "early" (AnVps34, AnVps19, and AnVps45) and "late" (CORVET) effectors (Figure 11), RabA seems unable to recruit the former and is a less efficient recruiter of CORVET. Simultaneous loss of RabB and RabA is lethal, indicating that they share some essential role, possibly involving LE biogenesis. This role might be related to hyphal growth, because the *digA1* truncating mutation in the gene encoding AnVps18 leads to the expected vacuolar fragmentation but also displays polarity maintenance (*dig* [dichotomous growth]) and nuclear distribution defects (Geissenhoner *et al.*, 2001).

Rab5 underwent duplication at the root of the fungal-metazoan branch. Thus the basic fungal set (*S. cerevisiae* Ypt51p-related Ypt53p is a recent acquisition deriving from a whole genome duplication) would involve RabA (Ypt52p) and RabB (Vps21/Ypt51p) (Pereira-Leal, 2008). Function suboptimization after gene duplication would explain the partial loss of Rab5 functions seen with RabA.

The SM protein AnVps45 and the FYVE protein AnVps19 are specific effectors of RabB. In *S. cerevisiae* the major target of Vps45p is the syntaxin Tlg2p, which plays roles both in the TGN and in an endosomal compartment functionally located at the interface with the *trans*-Golgi (Nichols *et al.*, 1998; Holthuis *et al.*, 1998a,b; Lewis *et al.*, 2000; Bryant and James, 2001). Genetic evidence showed that Tlg2p cannot be the sole target of Vps45p, and indeed Vps45p is involved in Golgi-to-endosomes traffic and pulls down the endosomal syntaxin Pep12p from extracts, indicating that it mediates regulation by Vps21p of Pep12p-dependent fusion events at prevacuolar endosomes (Cowles *et al.*, 1994; Horazdovsky *et al.*, 1994; Webb *et al.*, 1997; Burd *et al.*, 1997; Nichols *et al.*, 1998; Bryant *et al.*, 1998; Peterson *et al.*, 1999). Our results suggest that *A. nidulans* RabB couples the Vps34-dependent biosynthesis of PI(3)P with acquisition of the Vps45-mediated competence to accept Golgi traffic and with CORVET-mediated endosomal maturation (Figure 11).

In *S. cerevisiae*, the Pep12p syntaxin mediates membrane fusion in prevacuolar endosomes, whereas another syntaxin, Vam3p, is involved in homotypic vacuolar fusion. *A. nidulans* lacks Vam3p, and thus AnPep12 is the only syntaxin

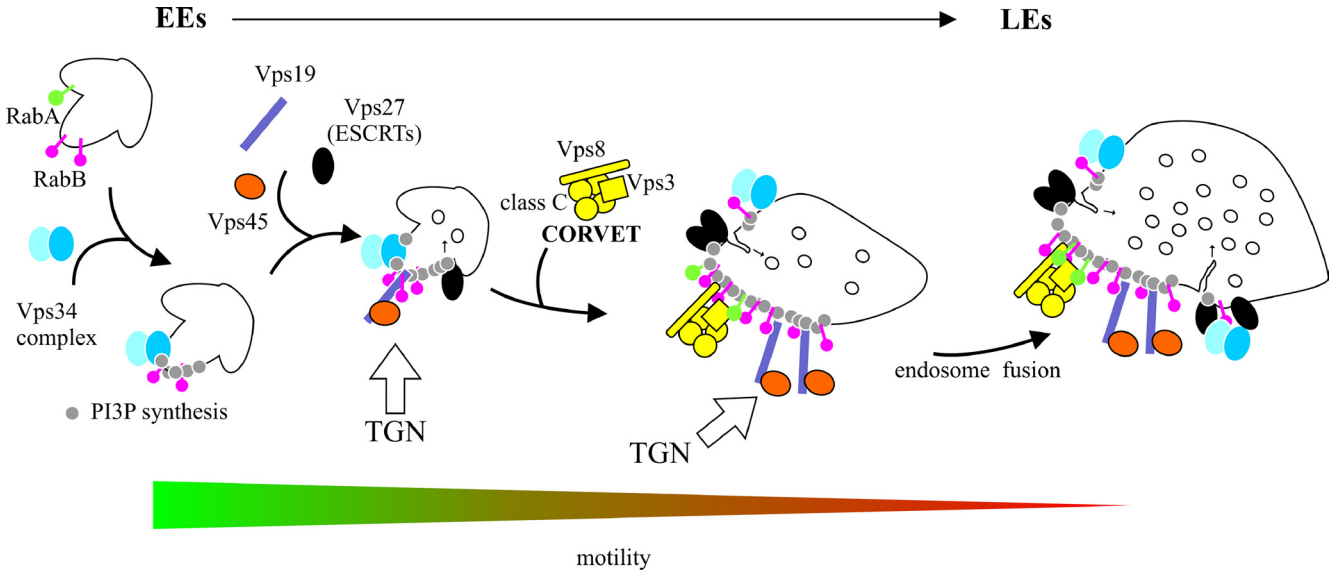

Figure 11. A model of *A. nidulans* EE maturation. After membrane recruitment of RabB and its activation by GTP, early endosomal domains acquire degradative identity because RabB-GTP (red lollypops) engages the Vps34 complex, which synthesizes PI(3)P (gray circles). This leads to subsequent recruitment to EEs of "early" effectors including the FYVE domain protein Vps19 and the SM protein Vps45, which mediate fusion of Golgi-derived traffic with endosomes. The also FYVE domain protein Vps27, the gatekeeper of the MVB pathway, is incorporated from this early stage, and primes ESCRT-I–, -II–, and -III–mediated inward vesicle budding (this work; motile early endosomes contain Vps32; see Galindo *et al.*, 2007). On formation of RabB domains, motile endosomes undergo long-distance movement on MTs. In a subsequent step, CORVET is recruited to Rab5 domains, mediating the Vps8-dependent fusion of endosomes as proposed (Markgraf *et al.*, 2009), which leads to a progressive increase in size with a concomitant loss of long-distance motility. Once endosomes reach a certain degree of maturation, Ypt7 replaces RabB (Vps21p), HOPS is exchanged for CORVET (Peplowska *et al.*, 2007), and LEs become competent to undergo homotypic fusion (not shown).

acting across the entire endocytic degradative pathway (Sánchez-Ferrero and Peñalva, 2006; Figure 11). *S. cerevisiae vps21*Δ shows a prototypic class D ("enlarged vacuole") phenotype (Raymond *et al.*, 1992). In contrast, *rabB*Δ results in vacuolar fragmentation. We speculate that the absence of an *A. nidulans* Vam3p orthologue underlies this phenotypic paradox. In yeast Vam3p reaches the vacuole directly from the Golgi (Cowles *et al.*, 1997). If AnPep12, the almost certain player of the Vam3p role, reaches the *A. nidulans* vacuole via endosomes, *rabB*Δ impairment of EE maturation would lead to inefficient AnPep12 traffic to the vacuole and deficient vacuolar fusion, thus resembling the fragmented vacuole phenotype of yeast *vam3*Δ mutants (Nichols *et al.*, 1997).

Long-distance motility of filamentous fungal EEs was first observed using *U. maydis* Yup1 SNARE, the *S. cerevisiae* Syn8p orthologue (Wedlich-Soldner *et al.*, 2000). Syn8p forms SNARE-pins containing Pep12p (Lewis and Pelham, 2002). Assuming that *U. maydis* Yup1 and *A. nidulans* RabB/RabA motile endosomes are equivalent, it follows that the latter contain both AnPep12 and the RabB effector AnVps45, which suggests that Golgi-derived traffic reaches the endosomal system from the early steps of the endocytic pathway. As noted, RabB mediates acquisition of PI(3)P. Like RabB, the AnVps27 FYVE domain decorates the motile population of endosomes, indicating that MVB sorting also takes place already at these early steps (Figure 11). Thus one attractive hypothesis is that traffic of EEs through the tip is coupled to sorting of cargoes into AnPep12/RabB degradative endosomes that move away from the tip as they progress to mature endosomes, thus resembling the process of mammalian endosomal maturation (Rink *et al.*, 2005).

An important finding of this work is that *A. nidulans* EE motility is dependent on RabB, which might mediate EE engagement to microtubule motors. As EEs circulate toward the plus ends before their loading on dynein, disrupting endosomal engagement to the plus end–directed motor would prevent movement in either direction. Kinesin KIF16B, mediating motility of mammalian EEs, contains a PI(3)P-binding PX domain (Hoepfner *et al.*, 2005). PI(3)P-mediated binding of *A. nidulans* EEs to a kinesin is an attractive possibility because it would explain why RabA, which does not recruit AnVps34, seems dispensable for motility. Kin3 and UncA kinesins mediating EE movement in *U. maydis* and *A. nidulans*, respectively (Wedlich-Soldner *et al.*, 2002; Zekert and Fischer, 2008), contain PH domains, which bind a broad number of partners (Lemmon, 2008). However, there is precedent of one fungal PH domain that binds PI(3)P on endosomes (Teo *et al.*, 2006). Thus, an attractive but as yet untested possibility is that the KinA/UncA PH domain recognizes PI(3)P, thus coupling acquisition of degradative endosomal identity with long-distance movement.

ACKNOWLEDGMENTS

We thank H. Arst for critical reading of the manuscript, E. Reoyo for technical assistance, S. Juárez and S. Ciordia for help with mass spectrometry, P. Pérez for advice on nucleotide-binding assays, and two anonymous referees for helpful suggestions. This work was supported by Spanish Ministry of Science and Innovation Grants BIO2006-556 and BIO2009-7281 to M.A.P. and by a Comunidad de Madrid Networking Grant SAL/0246/2006 (C.G. and M.A.P.). J.F.A., A.G., and A.P. were supported by Consejo Superior de Investigaciones Cientificas I3P, Formación de Personal Universitario, and Federation of European Biochemical Societies fellowships, respectively.

REFERENCES

Abenza, J. F., Pantazopoulou, A., Rodríguez, J. M., Galindo, A., and Peñalva, M. A. (2009). Long-distance movement of *Aspergillus nidulans* early endosomes on microtubule tracks. Traffic *10*, 57–75.

Aniento, F., Emans, N., Griffiths, G., and Gruenberg, J. (1993). Cytoplasmic dynein-dependent vesicular transport from early to late endosomes. J. Cell Biol. *123*, 1373–1387.

Apostolaki, A., Erpapazoglou, Z., Harispe, L., Billini, M., Kafasla, P., Kizis, D., Peñalva, M. A., Scazzocchio, C., and Sophianopoulou, V. (2009). AgtA, the dicarboxylic amino acid transporter of *Aspergillus nidulans*, is concertedly down-regulated by exquisite sensitivity to nitrogen metabolite repression and ammonium-elicited endocytosis. Eukaryot. Cell *8*, 339–352.

Bilodeau, P. S., Urbanowski, J. L., Winistorfer, S. C., and Piper, R. C. (2002). The Vps27p Hse1p complex binds ubiquitin and mediates endosomal protein sorting. Nat. Cell Biol. *4*, 534–539.

Bryant, N. J., and James, D. E. (2001). Vps45p stabilizes the syntaxin homologue Tlg2p and positively regulates SNARE complex formation. EMBO. J. *20*, 3380–3388.

Bryant, N. J., Piper, R. C., Gerrard, S. R., and Stevens, T. H. (1998). Traffic into the prevacuolar/endosomal compartment of *Saccharomyces cerevisiae*: a VPS45-dependent intracellular route and a VPS45-independent, endocytic route. Eur. J. Cell Biol. *76*, 43–52.

Burd, C. G., and Emr, S. D. (1998). Phosphatidylinositol(3)-phosphate signaling mediated by specific binding to RING FYVE domains. Mol. Cell *2*, 157–162.

Burd, C. G., Peterson, M., Cowles, C. R., and Emr, S. D. (1997). A novel Sec18p/NSF-dependent complex required for Golgi-to-endosome transport in yeast. Mol. Biol. Cell *8*, 1089–1104.

Calcagno-Pizarelli, A. M., *et al.* (2007). Establishment of the ambient pH signaling complex in *Aspergillus nidulans*: PalI assists plasma membrane localization of PalH. Eukaryot. Cell *6*, 2365–2375.

Christoforidis, S., McBride, H. M., Burgoyne, R. D., and Zerial, M. (1999a). The Rab5 effector EEA1 is a core component of endosome docking. Nature *397*, 621–625.

Christoforidis, S., Miaczynska, M., Ashman, K., Wilm, M., Zhao, L., Yip, S. C., Waterfield, M. D., Backer, J. M., and Zerial, M. (1999b). Phosphatidylinositol-3-OH kinases are Rab5 effectors. Nat. Cell Biol. *1*, 249–252.

Christoforidis, S., and Zerial, M. (2000). Purification and identification of novel Rab effectors using affinity chromatography. Methods *20*, 403–410.

Cowles, C. R., Emr, S. D., and Horazdovsky, B. F. (1994). Mutations in the *VPS45* gene, a *SEC1* homologue, result in vacuolar protein sorting defects and accumulation of membrane vesicles. J. Cell Sci. *107*, 3449–3459.

Cowles, C. R., Odorizzi, G., Payne, G. S., and Emr, S. D. (1997). The AP-3 adaptor complex is essential for cargo-selective transport to the yeast vacuole. Cell *91*, 109–118.

Galindo, A., Hervás-Aguilar, A., Rodríguez-Galán, O., Vincent, O., Arst, H. N., Jr., Tilburn, J., and Peñalva, M. A. (2007). PalC, one of two Bro1 domain proteins in the fungal pH signaling pathway, localizes to cortical structures and binds Vps32. Traffic *8*, 1346–1364.

Gaullier, J. M., Simonsen, A., D'Arrigo, A., Bremnes, B., Stenmark, H., and Aasland, R. (1998). FYVE fingers bind PtdIns(3)P. Nature *394*, 432–433.

Geissenhoner, A., Sievers, N., Brock, M., and Fischer, R. (2001). *Aspergillus nidulans* DigA, a potential homolog of *Saccharomyces cerevisiae* Pep3 (Vps18), is required for nuclear migration, mitochondrial morphology and polarized growth. Mol. Genet. Genom. *266*, 672–685.

Hama, H., Tall, G. G., and Horazdovsky, B. F. (1999). Vps9p is a guanine nucleotide exchange factor involved in vesicle-mediated vacuolar protein transport. J. Biol. Chem. *274*, 15284–15291.

Hervás-Aguilar, A., Rodríguez, J. M., Tilburn, J., Arst, H. N., Jr., and Peñalva, M. A. (2007). Evidence for the direct involvement of the proteasome in the proteolytic processing of the *Aspergillus nidulans* zinc finger transcription factor PacC. J. Biol. Chem. *282*, 34735–34747.

Hoepfner, S., Severin, F., Cabezas, A., Habermann, B., Runge, A., Gillooly, D., Stenmark, H., and Zerial, M. (2005). Modulation of receptor recycling and degradation by the endosomal kinesin KIF16B. Cell *121*, 437–450.

Holthuis, J. C., Nichols, B. J., Dhruvakumar, S., and Pelham, H. R. (1998a). Two syntaxin homologues in the TGN/endosomal system of yeast. EMBO J. *17*, 113–126.

Holthuis, J. C., Nichols, B. J., and Pelham, H. R. (1998b). The syntaxin Tlg1p mediates trafficking of chitin synthase III to polarized growth sites in yeast. Mol. Biol. Cell *9*, 3383–3397.

Horazdovsky, B. F., Busch, G. R., and Emr, S. D. (1994). VPS21 encodes a rab5-like GTP binding protein that is required for the sorting of yeast vacuolar proteins. EMBO J. *13*, 1297–1309.

Horiuchi, H., *et al.* (1997). A novel Rab5 GDP/GTP exchange factor complexed to Rabaptin-5 links nucleotide exchange to effector recruitment and function. Cell *90*, 1149–1159.

Katzmann, D. J., Stefan, C. J., Babst, M., and Emr, S. D. (2003). Vps27 recruits ESCRT machinery to endosomes during MVB sorting. J. Cell Biol. *162*, 413–423.

Kihara, A., Noda, T., Ishihara, N., and Ohsumi, Y. (2001). Two distinct Vps34 phosphatidylinositol 3-kinase complexes function in autophagy and carboxypeptidase Y sorting in *Saccharomyces cerevisiae*. J. Cell Biol. *152*, 519–530.

Lemmon, M. A. (2008). Membrane recognition by phospholipid-binding domains. Nat. Rev. Mol. Cell Biol. *9*, 99–111.

Lenz, J. H., Schuchardt, I., Straube, A., and Steinberg, G. (2006). A dynein loading zone for retrograde endosome motility at microtubule plus-ends. EMBO J. *25*, 2275–2286.

Lewis, M. J., Nichols, B. J., Prescianotto-Baschong, C., Riezman, H., and Pelham, H. R. (2000). Specific retrieval of the exocytic SNARE Snc1p from early yeast endosomes. Mol. Biol. Cell *11*, 23–38.

Lewis, M. J., and Pelham, H. R. (2002). A new yeast endosomal SNARE related to mammalian syntaxin 8. Traffic *3*, 922–929.

Markgraf, D. F., Ahnert, F., Arlt, H., Mari, M., Peplowska, K., Epp, N., Griffith, J., Reggiori, F., and Ungermann, C. (2009). The CORVET subunit Vps8 cooperates with the Rab5 homolog Vps21 to induce clustering of late endosomal compartments. Mol. Biol. Cell *20*, 5276–5289.

Nayak, T., Szewczyk, E., Oakley, C. E., Osmani, A., Ukil, L., Murray, S. L., Hynes, M. J., Osmani, S. A., and Oakley, B. R. (2005). A versatile and efficient gene targeting system for *Aspergillus nidulans*. Genetics *172*, 1557–1566.

Nichols, B. J., Holthuis, J. C., and Pelham, H. R. (1998). The Sec1p homologue Vps45p binds to the syntaxin Tlg2p. Eur. J. Cell Biol. *77*, 263–268.

Nichols, B. J., Ungermann, C., Pelham, H. R., Wickner, W. T., and Haas, A. (1997). Homotypic vacuolar fusion mediated by t- and v-SNAREs. Nature *387*, 199–202.

Nielsen, E., Christoforidis, S., Uttenweiler-Joseph, S., Miaczynska, M., Dewitte, F., Wilm, M., Hoflack, B., and Zerial, M. (2000). Rabenosyn-5, a novel Rab5 effector, is complexed with hVPS45 and recruited to endosomes through a FYVE finger domain. J. Cell Biol. *151*, 601–612.

Nielsen, E., Severin, F., Backer, J. M., Hyman, A. A., and Zerial, M. (1999). Rab5 regulates motility of early endosomes on microtubules. Nat. Cell Biol. *1*, 376–382.

Ohsumi, K., Arioka, M., Nakajima, H., and Kitamoto, K. (2002). Cloning and characterization of a gene (*avaA*) from *Aspergillus nidulans* encoding a small GTPase involved in vacuolar biogenesis. Gene *291*, 77–84.

Pantazopoulou, A., and Peñalva, M. A. (2009). Organization and dynamics of the *Aspergillus nidulans* Golgi during apical extension and mitosis. Mol. Biol. Cell *20*, 4335–4347.

Peñalva, M. A. (2005). Tracing the endocytic pathway of *Aspergillus nidulans* with FM4-64. Fungal Genet. Biol. *42*, 963–975.

Peplowska, K., Markgraf, D. F., Ostrowicz, C. W., Bange, G., and Ungermann, C. (2007). The CORVET tethering complex interacts with the yeast Rab5 homolog Vps21 and is involved in endo-lysosomal biogenesis. Dev. Cell *12*, 739–750.

Pereira-Leal, J. B. (2008). The Ypt/Rab family and the evolution of trafficking in fungi. Traffic *9*, 27–38.

Peterson, M. R., Burd, C. G., and Emr, S. D. (1999). Vac1p coordinates Rab and phosphatidylinositol 3-kinase signaling in Vps45p-dependent vesicle docking/fusion at the endosome. Curr. Biol. *9*, 159–162.

Prag, G., Watson, H., Kim, Y. C., Beach, B. M., Ghirlando, R., Hummer, G., Bonifacino, J. S., and Hurley, J. H. (2007). The Vps27/Hse1 complex is a GAT domain-based scaffold for ubiquitin-dependent sorting. Dev. Cell *12*, 973–986.

Raymond, C. K., Howald-Stevenson, I., Vater, C. A., and Stevens, T. H. (1992). Morphological classification of the yeast vacuolar protein sorting mutants: evidence for a prevacuolar compartment in class E vps mutants. Mol. Biol. Cell *3*, 1389–1402.

Rink, J., Ghigo, E., Kalaidzidis, Y., and Zerial, M. (2005). Rab conversion as a mechanism of progression from early to late endosomes. Cell *122*, 735–749.

Rodríguez-Galán, O., Galindo, A., Hervás-Aguilar, A., Arst, H. N., Jr., and Peñalva, M. A. (2009). Physiological involvement in pH signalling of Vps24-mediated recruitment of *Aspergillus* PalB cysteine protease to ESCRT-III. J. Biol. Chem. *284*, 4404–4412.

Sánchez-Ferrero, J. C., and Peñalva, M. A. (2006). Endocytosis. In: The *Aspergilli:* Genomics, Medical Aspects, Biotechnology, and Research Methods, ed. G. H. Goldman and S.A. Osmani, Boca Ratón, FL: CRC Press, 177–195.

Sato, T. K., Rehling, P., Peterson, M. R., and Emr, S. D. (2000). Class C Vps protein complex regulates vacuolar SNARE pairing and is required for vesicle docking/fusion. Mol. Cell *6*, 661–671.

Seals, D. F., Eitzen, G., Margolis, N., Wickner, W. T., and Price, A. (2000). A Ypt/Rab effector complex containing the Sec1 homolog Vps33p is required for homotypic vacuole fusion. Proc. Natl. Acad. Sci. USA *97*, 9402–9407.

Shevchenko, A., Tomas, H., Havlis, J., Olsen, J. V., and Mann, M. (2006). In-gel digestion for mass spectrometric characterization of proteins and proteomes. Nat. Protoc. *1*, 2856–2860.

Simonsen, A., Lippe, R., Christoforidis, S., Gaullier, J. M., Brech, A., Callaghan, J., Toh, B. H., Murphy, C., Zerial, M., and Stenmark, H. (1998). EEA1 links PI(3)K function to Rab5 regulation of endosome fusion. Nature *394*, 494–498.

Singer-Kruger, B., Stenmark, H., Dusterhoft, A., Philippsen, P., Yoo, J. S., Gallwitz, D., and Zerial, M. (1994). Role of three rab5-like GTPases, Ypt51p, Ypt52p, and Ypt53p, in the endocytic and vacuolar protein sorting pathways of yeast. J. Cell Biol. *125*, 283–298.

Siniossoglou, S. (2005). Affinity purification of Ypt6 effectors and identification of TMF/ARA160 as a Rab6 interactor. Methods Enzymol. *403*, 599–607.

Steinberg, G. (2007). On the move: endosomes in fungal growth and pathogenicity. Nat. Rev. Microbiol. *5*, 309–316.

Subramanian, S., Woolford, C. A., and Jones, E. W. (2004). The Sec1/Munc18 protein, Vps33p, functions at the endosome and the vacuole of *Saccharomyces cerevisiae.* Mol. Biol. Cell *15*, 2593–2605.

Szewczyk, E., Nayak, T., Oakley, C. E., Edgerton, H., Xiong, Y., Taheri-Talesh, N., Osmani, S. A., and Oakley, B. R. (2006). Fusion PCR and gene targeting in *Aspergillus nidulans.* Nat. Protoc. *1*, 3111–3120.

Taheri-Talesh, N., Horio, T., Araujo-Bazán, L., Dou, X., Espeso, E. A., Peñalva, M. A., Osmani, S. A., and Oakley, B. R. (2008). The tip growth apparatus of *Aspergillus nidulans.* Mol. Biol. Cell *19*, 1439–1449.

Tall, G. G., Hama, H., DeWald, D. B., and Horazdovsky, B. F. (1999). The phosphatidylinositol 3-phosphate binding protein Vac1p interacts with a Rab GTPase and a Sec1p homologue to facilitate vesicle-mediated vacuolar protein sorting. Mol. Biol. Cell *10*, 1873–1889.

Teo, H., Gill, D. J., Sun, J., Perisic, O., Veprintsev, D. B., Vallis, Y., Emr, S. D., and Williams, R. L. (2006). ESCRT-I core and ESCRT-II GLUE domain structures reveal role for GLUE in linking to ESCRT-I and membranes. Cell *125*, 99–111.

Valdez-Taubas, J., and Pelham, H. R. (2003). Slow diffusion of proteins in the yeast plasma membrane allows polarity to be maintained by endocytic cycling. Curr. Biol. *13*, 1636–1640.

Webb, G. C., Zhang, J., Garlow, S. J., Wesp, A., Riezman, H., and Jones, E. W. (1997). Pep7p provides a novel protein that functions in vesicle-mediated transport between the yeast Golgi and endosome. Mol. Biol. Cell *8*, 871–895.

Wedlich-Soldner, R., Bolker, M., Kahmann, R., and Steinberg, G. (2000). A putative endosomal t-SNARE links exo- and endocytosis in the phytopathogenic fungus *Ustilago maydis.* EMBO J. *19*, 1974–1986.

Wedlich-Soldner, R., Straube, A., Friedrich, M. W., and Steinberg, G. (2002). A balance of KIF1A-like kinesin and dynein organizes early endosomes in the fungus *Ustilago maydis.* EMBO J. *21*, 2946–2957.

Zekert, N., and Fischer, R. (2008). The *Aspergillus nidulans* kinesin-3 UncA motor moves vesicles along a subpopulation of microtubules. Mol. Biol. Cell *20*, 673–684.

Zerial, M., and McBride, H. (2001). Rab proteins as membrane organizers. Nat. Rev. Mol. Cell Biol. *2*, 107–117.